Journal of Cleaner Production 436 (2024) 140530

Contents lists available at ScienceDirect

Journal of Cleaner Production

journal homepage: www.elsevier.com/locate/jclepro

Offshore wind farm site selection in Norway: Using a fuzzy trigonometric weighted assessment model

Umit Cali [a,b], Emre Kantar [c,*], Dragan Pamucar [d,e], Muhammet Deveci [f,g], Peter Taylor [h], David Campos-Gaona [h], Olimpo Anaya-Lara [a,h], John O. Tande [i]

[a] Department of Electric Energy Norwegian University of Science and Technology, Trondheim, Norway
[b] School of Physics, Engineering and Technology, University of York, York, United Kingdom
[c] Department of Electric Power Technology, SINTEF Energy Research, Trondheim, Norway
[d] Faculty of Organizational Sciences, University of Belgrade, Belgrade, Serbia
[e] College of Engineering, Yuan Ze University, Taoyuan, Taiwan
[f] Department of Industrial Engineering, Turkish Naval Academy, National Defence University, Istanbul, Turkey
[g] The Bartlett School of Sustainable Construction, University College London, London, United Kingdom
[h] Department of Electronic and Electrical Engineering, University of Strathclyde, Glasgow, United Kingdom
[i] Department of Energy Systems, SINTEF Energy Research, Trondheim, Norway

ARTICLE INFO

Handling Editor: Xin Tong

Keywords:
Renewable energy
Offshore wind farm
Site selection
Multi-criteria decision-making
Fuzzy trigonometric weighted assessment
Ordinal Priority Approach

ABSTRACT

Maximising the energy potential of offshore wind farms requires an in-depth assessment of technological, economic, sociopolitical, and environmental aspects. Given the large economic impact of large-scale projects, a robust site selection procedure is critical for limiting financial risks while supporting informed investments. This research uncovers a novel and multidisciplinary approach for boosting the efficacy of Norwegian and global offshore wind farm siting investments. The proposed method uses a two-stage fuzzy mathematical model that considers technical, economic, logistical, and environmental factors. It combines the Ordinal Priority Approach (F-OPA) and Trigonometric Weighted Assessment (TRWA) technique by using an in-depth techno-economic assessment. An alternative reactive power compensation model, power loss calculations, and associated techno-economic analysis were performed for the investigated offshore wind farm locations. Furthermore, the energy economic calculations are carried out to provide support for the proposed decision-making framework. The proposed methodology was tested through a case study, focusing on ranking Norwegian offshore wind farm sites selected from potential locations announced by The Norwegian Water Resources and Energy Directorate (NVE). Within the Norwegian offshore wind farm sites, the approach demonstrated a versatile and efficient decision-making process at both individual and collective levels, identifying the Sandskallen-Sørøya Nord project as a pivotal investment priority and providing valuable managerial insights to enhance Norway's offshore wind initiatives. The model's stability was affirmed through a sensitivity analysis, underscoring its potential to enhance renewable energy policy and decision-making globally.

1. Introduction

The increasing global demand for energy, coupled with the need to mitigate climate change, has led to a growing interest in offshore wind power as a viable source of renewable energy. Also, decarbonisation has been one of the main trends for modern energy systems for two decades. Wind power is one of the main drivers of decarbonisation globally. Wind energy economics has emerged as a pivotal aspect of the renewable energy sector, as the industry's growth depends heavily on its financial viability (IRENA, 2020). In recent years, offshore wind projects have become technically and economically feasible in various regions of the world. The development of offshore wind farms, particularly in regions with favourable wind conditions, has become a promising solution to meet the increasing energy demand while reducing carbon emissions. As wind energy technology advances and economies of scale are achieved, the industry has observed significant reductions in Capital Expenditure (CAPEX), Operational Expenditure (OPEX), and Levelised Cost of Energy (LCOE), making offshore wind

* Corresponding author.
E-mail addresses: umit.cali@ntnu.no (U. Cali), emre.kantar@sintef.no (E. Kantar), dpamucar@gmail.com (D. Pamucar), muhammetdeveci@gmail.com (M. Deveci), peter.taylor@strath.ac.uk (P. Taylor), d.campos-gaona@strath.ac.uk (D. Campos-Gaona), olimpo.anaya-lara@ntnu.no, olimpo.anaya-lara@strath.ac.uk (O. Anaya-Lara), john.o.tande@sintef.no (J.O. Tande).

https://doi.org/10.1016/j.jclepro.2023.140530
Received 20 July 2023; Received in revised form 6 December 2023; Accepted 30 December 2023
Available online 2 January 2024

List of Abbreviations

AEY	Annual Energy Yield
AHP	Analytic Hierarchy Process
BWM	Best-Worst Method
CAPEX	Capital Expenditure
CF	Capacity Factor
CoCoSo	Combined Compromised Solution
FOWTs	Floating Offshore Wind Turbines
FUCOM	Full Consistency Method
GIS	Geographic Information System
I2TL	Interval 2-Tuple Linguistic
LCOE	Levelised Cost of Energy
MABAC	Multi-Attributive Border Approximation Area Comparison
MCDM	Multi-Criteria Decision-Making
MERRA-2	The Modern-Era Retrospective Analysis for Research and Applications Version 2
NVE	The Norwegian Water Resources and Energy Directorate
OPA	Ordinal Priority Approach
OPEX	Operational Expenditure
OWF	Offshore Wind Farm
TRWA	Fuzzy Trigonometric Weighted Assessment
WASPAS	Weighted Aggregated Sum Product Assessment
WPM	Weighted Product Model WSM Weighted Sum Model

energy increasingly competitive with traditional energy sources. Evaluating these financial parameters is crucial for policymakers, investors, and researchers to determine the attractiveness and sustainability of wind energy projects in the global energy landscape (DOE, 2020; Lazard, 2020; Maienza et al., 2020; Shields et al., 2021).

European countries, in particular, set various ambitious targets to fulfil the international and national sustainability-related conventions (DNV, 2023). In response to the call from last year's climate summit for all countries to reevaluate their emission reduction targets, Norway will aim to cut emissions by at least 55% by 2030, compared to the 1990 level, with offshore wind energy expected to play a significant role in achieving this target (Norwegian Government, 2023). Offshore wind has started to be an integral part of such energy policy targets. Therefore, governments have developed considerable support mechanisms to subsidise offshore developments in their countries because offshore wind projects usually have higher CAPEX and OPEX values, which directly impact the main techno-economic indicators such as LCOE, amortisation times, and other relevant metrics.

The development of offshore wind farms requires careful site selection to ensure that environmental, technical, and economic factors are taken into consideration. Dedicated methods are required for accurately processing the diverse qualitative parameters, such as impact on marine life and legislative focus, and quantitative parameters, such as capacity factor, annual energy yield, and wind speed. These parameters are closely intertwined with the development and operation of offshore wind energy projects due to the inherently complex and interdisciplinary nature of investment decision-making in these projects.

While substantial research has been undertaken in the field of offshore wind resource exploration and consolidation, studies focusing on the site selection for an Offshore Wind Farm (OWF) remain limited. Prior studies on offshore wind energy research emphasise the need for sustainable and effective solutions to boost energy output and cost-effectiveness (Abdel-Basset et al., 2021; Zhang et al., 2018). The numerous constraints inherent in the process of siting OWF often lead to the formulation of this task as a strategic Multi-Criteria Decision-Making (MCDM) problem (Yu et al., 2022a; Li et al., 2022; Yu et al., 2022b; Yazdi et al., 2022; Wang et al., 2022; Deveci et al., 2022; Rani et al., 2019; Adedeji et al., 2020). Techniques for operation and maintenance are crucial in determining an optimal solution.

However, most of the earlier research did not adopt a holistic approach. The existing corpus of knowledge on offshore wind energy systems has several crucial gaps, such as:

- Insufficient investigations of comprehensive and interdisciplinary approaches that integrate economics, technology, renewable energy strategies, socio-political perspectives, and environmental science.
- A lack of focus on nuanced factors crucial for the feasibility and effectiveness of offshore wind energy systems, such as detailed power loss calculations and cost-related inherent complexities.
- Inadequate use of advanced decision-support tools and probabilistic uncertainty modelling to tackle complex issues such as the disparity between the ability to handle uncertainty and the convenience of usage, insufficient consideration of individual variances, and incomplete criterion weights (Yin et al., 2021).

Considering these identified gaps in the literature, this study poses the following research question: "*How can a holistic decision-making framework enhance decision-making for the evaluation and prioritisation of OWF sites, thereby advancing offshore wind energy initiatives, energy sustainability, and climate mitigation efforts?*"

To address this research question, the primary objective of this study is to develop a novel multi-criteria decision-making framework, specifically tailored to address the multifaceted challenges inherent in OWF siting. This framework aims to enhance decision-making by adeptly managing expert uncertainties and biases and effectively handling undetermined or uncertain data, thereby contributing to the advancement of offshore wind energy.

1.1. Scope of Norway-specific decision-making framework

A holistic decision-making support framework is developed using a novel fuzzy mathematical model for multi-attribute decision-making, which is based on the application of two modules. The first module is based on the application of the Ordinal Priority Approach (OPA) method (Ataei et al., 2020) in a fuzzy environment (F-OPA) and is used to determine the weight coefficients of the criteria. The second module is based on applying fuzzy non-linear functions of sine trigonometry for evaluating alternatives.

The proposed F-OPA algorithm linear model enables the flexible, objective, and rational processing of uncertain and undetermined information as well as expert uncertainty and bias. A Fuzzy Trigonometric Weighted Assessment (TRWA) methodology is developed for the objective representation of information in the initial decision matrix. Non-linear fuzzy trigonometric functions are based on the implementation of trigonometric norms in traditional aggregation functions (Hu et al., 2015). A multi-criteria model is thus generated by introducing trigonometric norms that enable flexible decision-making and the presentation of uncertainty and risk when making decisions. The rationale for using the F-OPA algorithm and TRWA is elaborated in Section 1.3.

The proposed algorithm is fed with both quantitative and qualitative data, spanning various dimensions, including energy, politics, legislation, technology, economics, social impacts, and environmental issues, all of which are detailed in Section 3.1. Special attention is devoted to addressing detailed power loss calculations, considering various factors such as array losses, wind turbine type, inter-array cabling, export cable, and reactive power compensation, alongside providing detailed calculations for CAPEX and OPEX.

A case study is used to rank the Norwegian offshore wind farm sites, selected from potential sites announced by The Norwegian Water Resources and Energy Directorate (NVE) (Berg et al., 2012). The reasons why the Norwegian offshore sites were chosen are given below.

The present multifaceted energy crisis, intensified by geopolitical tensions and global inflation, is stressing conventional energy resources, leading to price hikes and supply disruptions. In this context, nations like Norway, with over 98% of their energy supplied from renewables, mainly hydroelectricity, stand as pillars of stability and sustainability. Norway's commitment to green energy safeguards it against fossil fuel market fluctuations and brands it as a potential green energy supplier to Europe. Unexploited offshore wind energy resources further enhance Norway's renewable capabilities. Strategic investments in such renewables enable Norway to diversify its energy mix, enhancing resilience and fulfilling global sustainability goals. Moreover, it could increase renewable energy exports to EU nations like Germany, addressing their energy crisis, benefiting Norway economically, and alleviating energy constraints in Europe. Norway's renewable surplus is pivotal for Europe's energy stability and pricing. Maximising offshore wind potential allows Norway to significantly counteract the impacts of energy crises and contributes to developing resilient and sustainable energy infrastructure in Europe. Norway's policy strength, environmental commitment, advanced infrastructure, public interest, innovation, and economic stability position it advantageously for tackling the challenges and opportunities of offshore wind projects.

1.2. Literature review on MCDM methodologies in offshore wind projects

Over the past decade, a substantial number of noteworthy research studies have emerged, focusing on various aspects of renewable energy, where diverse MCDM methodologies and integrated approaches have demonstrated considerable efficacy and adaptability in addressing complex site selection and optimisation challenges across a range of global contexts.

Yu et al. (2022a) introduced a novel integrated MCDM framework, based on the Interval 2-Tuple Linguistic (I2TL), to address the challenges of site selection in contexts characterised by uncertainty and incomplete information. Li et al. (2022) focused on optimising maintenance strategies for offshore wind farms, presenting a multi-objective model that balances the trade-off between the availability of wind turbines and the cost of maintenance, considering various factors, including failure rates and maintenance durations. Their approach provides a systematic and comprehensive framework, allowing for more effective and economically efficient maintenance strategies, which is crucial for the operational optimisation and long-term sustainability of offshore wind energy projects. Yu et al. (2022b), in another study, investigated a novel MCDM framework that aligns with human thinking logic demonstrated through a case study in China. The use of MCDM in their work has advanced this field by employing sophisticated methods to provide a comprehensive and quantifiable evaluation system. They claimed that uncertainties and different risk preferences create complex decision-making situations where the Combined Compromised Solution (CoCoSo) method was integrated with prospect theory to rank the alternatives in order of priority. Zhang et al. (2022) presented a systematic analysis of the performance and cost of two floating offshore wind turbines with significant interactions. The study focused on the energy production and LCOE for these turbines, taking into account the hydro-aerodynamics interaction. As per Zhang et al. (2022), due to the exhaustion of shallow water wind energy resources and the maturity of Floating Offshore Wind Turbines (FOWTs), the move from fixed-bottom to floating offshore wind technology is imminent. In the book chapter by Yazdi et al. (2022), a thorough review is provided, encompassing various MCDM methodologies employed for evaluating potential sites for installing offshore wind turbines.

The study by Wang et al. (2022) delved into the multifaceted considerations involved in Offshore Wind Power Station (OWPS) site selection, employing a comprehensive and integrative approach that amalgamates the CoCoSo method and Prospect Theory to assess and prioritise alternatives effectively. The approach enables a nuanced understanding and assessment of various influential factors, allowing for more informed and strategic decision-making in the field of renewable energy site selection, with implications for enhancing the sustainability and efficacy of offshore wind power development and contributing to more robust and reliable site selection processes in offshore wind power projects. In our earlier work Deveci et al. (2022), we investigated efficient q-rung orthopair fuzzy sets (q-ROFSs) based on the Full Consistency Method (FUCOM) and CoCoSo method for solving the floating OWF site selection problem in Norway for four different offshore sites. The analysis in Deveci et al. (2022) laid the groundwork for this study. It used fewer decision-making variables compared to the approach presented here (as will be shown in Section 3) and provided generalised, coarse calculations for factors such as electrical, array, and wake losses, as well as CAPEX and OPEX, rather than specific calculations for each site.

Krishankumar et al. (2021) explored solutions to renewable energy source selection problems by implementing a hybrid approach that combines Multiple Attribute Decision-Making (MADM) with grey relational analysis to evaluate and prioritise various renewable energy alternatives. The innovative methodology contributes to the field by addressing the complexities and uncertainties inherent in renewable energy source selection, offering a more structured and reliable framework for decision-makers in the renewable energy sector. Rani et al. (2019) introduced a novel VIKOR method, incorporating entropy and divergence measures, to address multiple criteria decision-making problems, especially emphasising intricate and conflicting criteria within the field of renewable energy source selection. This refined approach ensures elevated precision and reliability in decision-making endeavours, tackling inherent uncertainties and complexities in assessing and ranking alternatives in the renewable energy sector. Adedeji et al. (2020) performed a mini-review emphasising the pivotal role of neuro-fuzzy resource forecasting in conjunction with Geographic Information System (GIS) and MCDM tools for optimising site suitability assessments in wind and solar energy projects. The review underscores the necessity for intelligent, adaptive neuro-fuzzy systems to refine resource variability understanding and investment viability, enriching the site selection process for renewable energy by effectively analysing and ranking various attributes and criteria. MCDM-based models have also been successfully integrated into other decision-making problems (Dağıstanlı, 2023; Gökalp et al., 2024; Dinçer et al., 2023).

1.3. Identifying MCDM model limitations and novelty of the proposed framework

In traditional MCDM models, such as the Multi-Attributive Border Approximation Area Comparison (MABAC) method (Pamučar and Ćirović, 2015), VIKOR method (Opricovic and Tzeng, 2004) and Weighted Aggregated Sum Product Assessment (WASPAS) method (Zavadskas et al., 2012), the evaluation of alternatives is based on a comparative assessment using a linear weighted aggregation of criteria values, which is performed using the Weighted Sum Model (WSM) or Weighted Product Model (WPM). In both WSM and WPM models, aggregation involves a straightforward combination of criteria weight values and standardised information. This method yields satisfactory results when the information in the initial decision matrix is uniform. However, extreme deviations in information at the most influential criterion values can cause disproportionate changes in the aggregated utility function, a consequence of the linear nature of the WSM function. Another limitation of the WSM and WPM approaches is their neglect of interaction between criteria, overlooking significant objective connections between pieces of information.

A decision support system is crucial for minimising the anomalies presented, thereby objectifying decisions in real and dynamic systems. Moreover, multi-criteria tools are anticipated to incorporate built-in algorithms that rationally examine the interactions between decision attributes.

Consequently, this paper introduces a novel fuzzy TRWA model designed for information processing in the multi-criteria decision-making process. The distinctive features of the TRWA model are delineated below, setting it apart from existing MCDM tools:

(i) The fuzzy TRWA method facilitates flexible nonlinear processing of complex and uncertain information in real-world applications; (ii) nonlinear fuzzy trigonometric functions enhance model flexibility, fostering more objective reasoning under dynamic conditions; (iii) the introduction of additional stabilisation parameters in the aggregation function further refines the model's flexibility; (iv) the fuzzy TRWA model possesses a unique information standardisation algorithm, maintaining the disposition of normalised values of benefit and cost criteria.

Currently, no research in existing literature introduces an MCDM tool that integrates trigonometric functions and the reverse sorting algorithm for standardising information in the decision matrix, which accurately represents information around the origin and provides a more objective representation of the decision-makers' preferences. Therefore, a logical objective of this study is to demonstrate the applicability of the TRWA model for information fusion and flexible, objective, and rational reasoning.

In addition to the TRWA model, this study proposes enhancements to the OPA model within a fuzzy environment. The conventional OPA model generates a linear model based on predetermined criteria ranks, a limitation that prevents the rational representation of the significance of criteria when their influences are nearly equivalent. For instance, utilising the traditional OPA algorithm forces experts to rank criteria A and B as of approximately equal importance, hindering the objective representation of their significance. This illustration reveals that the conventional OPA model lacks the capability to represent the proximity between criteria, relying instead on a crude ranking for significance assessment. Hence, this study introduces refinements to the OPA model, enabling the importance evaluations of criteria to be defined through actual expert assessments.

The improved F-OPA model presented herein mitigates deviations from expert preferences inherent in other subjective models, including the Best-Worst Method (BWM) (Rezaei, 2015) and Analytic Hierarchy Process (AHP) (Saaty, 2008), as the outcomes of the enhanced OPA are invariably consistent. The rising inconsistencies in BWM and AHP evaluations often lead to the overshadowing of expert preferences, potentially resulting in erroneous decisions. Such issues with the mentioned methods stem from the utilisation of a predefined framework with a limited value range, hindering the rational representation of expert preferences (Mukhametzyanov, 2023; Bonab et al., 2023). Beyond the aforementioned attributes, the refined F-OPA model offers flexibility and resolves inconsistencies in the paired comparison technique. Furthermore, it allows for the processing of uncertain and ambiguous information, as well as the definition of weighting coefficients of criteria in cases of incomplete information regarding specific attributes, rendering it suitable for deployment in dynamic and uncertain environments.

1.4. Main contributions

The main contributions of this study are outlined below:

- Performance of in-depth power system analysis supported by detailed power loss calculations on an alternative reactive power compensation model design.
- Demonstration of tailored techno-economic assessment that combines detailed power systems analysis results and site-specific energy economic calculations.
- Introduction of an original non-linear aggregation function in the fuzzy TRWA model, allowing for a flexible assessment of the influence of weighted sequences (strategies). This proposed aggregation function enables the exploration and simulation of different levels of risk through various scenarios.
- Amalgamation of state-of-the-art decision-making methods such as the TRWA model, offshore-site-specific detailed techno-economic analysis, and other interdisciplinary criteria to yield the best feasible investment decisions to support informed decisions for investors and energy policy-makers.

1.5. Outline

In the following sections, we first provide background information related to OWF foundations and wind power. Subsequently, the methodology section encompasses the decision-making parameters, the alternative OWF sites, wind power calculations, and economic considerations. These decision-making parameters address various factors, including electrical, array and wake losses, CAPEX, OPEX, and the export cable for each OWF site, among others. Following the methodology, the mathematical background of the selected decision-making framework is elucidated. Experimental results are then presented, with discussions centred around the output of the fuzzy TRWA model. The conclusion summarises the main findings and discusses their policy implications.

2. Background

Background information for the types of recent Offshore Wind Turbines' (OWT) foundations and their share in today's market are briefly discussed here. In addition, the overall efficiency of a wind turbine, considering the sources of the losses, will be presented in this work, along with our assumptions for further analysis.

2.1. Offshore wind turbine foundations

Offshore wind turbine foundations are a crucial component of offshore wind farm design and play a critical role in the structural integrity, performance, and maintenance requirements of wind turbines. In general, offshore wind turbine foundations can be classified into two main categories: bottom-fixed and floating foundations, as illustrated in Fig. 1.

Bottom-fixed foundations can be further classified into monopile, jacket, and tripod. Gravity-based and monopile foundations are typically used in shallow waters (up to 35 m) and consist of a large steel tube driven into the seabed (Van der Valk, 2014). Its simplicity and robustness make the monopile foundation the preferred option for shallow waters (Beuckelaers, 2017).

Jacket foundations, on the other hand, are suitable for deeper waters (30–80 m) and consist of a lattice structure with multiple legs that provide support to the turbine. Tripod foundations are a variant of jacket foundations and have three legs that are inclined towards each other.

Floating foundations, an emerging technology, enable the deployment of wind turbines in even deeper waters. These foundations use a buoyant platform that is tethered to the seabed, allowing the turbine to float above the water surface. Floating foundations can be further classified into several types, including tension leg platforms, semi-submersible, and spar platforms, as illustrated in Fig. 1. Floating foundations start to become more and more competitive with the bottom-fixed foundations at waters around 50 m water deep and more feasible over bottom-fixed solutions at waters deeper than 60 m based on the future cost prognosis performed by Multiconsult in an optimistic scenario (Multiconsult, 2012), as shown in Fig. 2.

The design of offshore wind turbine foundations must take into account a range of technical and environmental factors, including

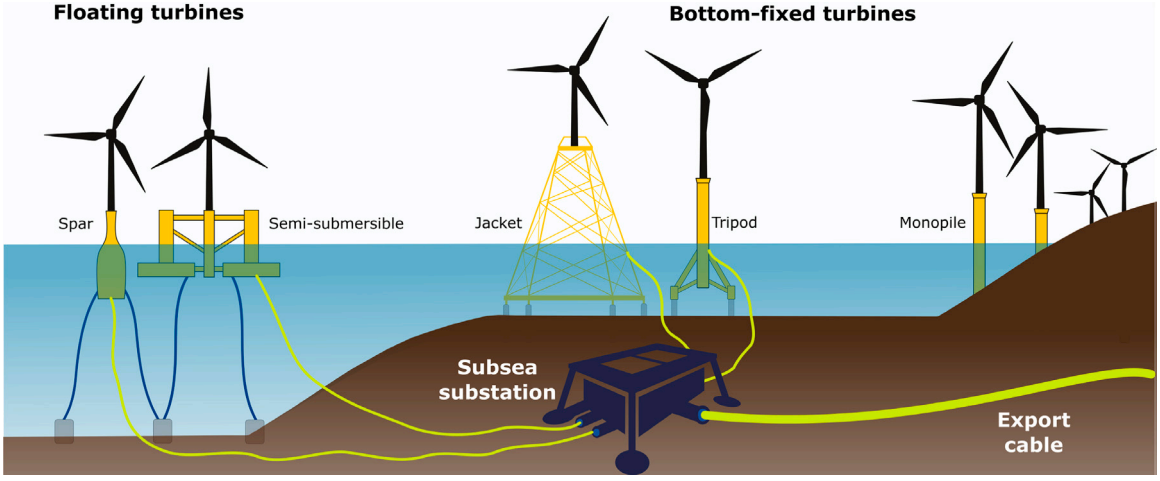

Fig. 1. Different foundation types for offshore wind turbines with bottom-fixed (jacket, tripod and monopile) and floating (spar and semi-submersible) foundations.

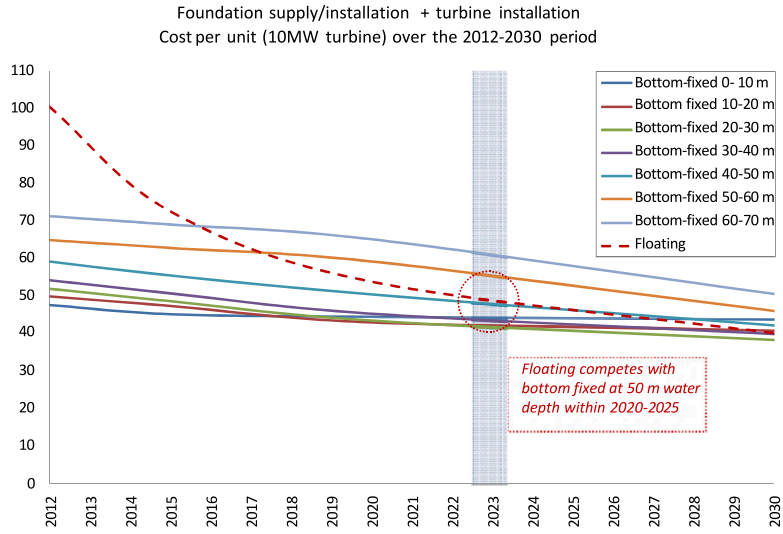

Fig. 2. Foundation supply/installation and 10 MW turbine installation cost comparison over the 2012–2030 period (optimistic scenario regarding cost reduction for floating) (Multiconsult, 2012).

wind and wave loads, soil conditions, and seabed topography. The foundation design must also consider the construction and installation methods, as well as the operational and maintenance requirements of the turbine.

As of today, floating offshore wind is a relatively new technology and currently represents a small fraction of the total installed capacity of offshore wind worldwide. According to the International Renewable Energy Agency (IRENA), as of the end of 2020, the total installed capacity of floating offshore wind was approximately 65 megawatts (MW), which is a very small percentage of the total installed capacity of offshore wind globally, which was approximately 31,000 MW (IRENA, 2021). However, there are numerous floating offshore wind projects in development and under construction, and many experts predict that the share of floating offshore wind will grow significantly in the coming years.

In summary, offshore wind turbine foundations are critical to the success of offshore wind farms, and their selection and design must be carefully considered to ensure the long-term performance and sustainability of these important energy resources. The choice of foundation type will depend on a range of factors, including water depth, seabed conditions, and environmental considerations. Bottom-fixed and floating foundations both have their own unique advantages and disadvantages, and their selection will depend on a range of technical, economic, and regulatory factors.

2.2. Wind power output

The average power that can be harvested from the wind (P_w), striking on a surface with area A (e.g., equal to the rotor swept area of a wind turbine [m^2]) is calculated by:

$$P_w = \frac{1}{2}\,\rho\,A\,v^3\,, \tag{1}$$

where ρ is the air density [kg/m^3], and v is the wind speed [m/s]. However, the theoretical limit to the maximum extracted power from the wind $P_{w,e}$ is 59.3%, according to Betz's law. Modern wind turbines can extract as much wind power as 45–50%, closing in on the theoretical limit (Dupont et al., 2018). One of the main loss mechanisms that determine $P_{w,e}$ are aerodynamic (turbine blades) and mechanical losses (gearbox, rotating parts, etc.) caused by the wind turbine. Wind power production is further inhibited as the placement of the turbines in a wind farm becomes sub-optimal for practical and feasibility reasons.

The capacity factor (CF) of a single wind turbine or small-scale wind farm cannot simply be extrapolated to a large wind farm that consists of tens or hundreds of wind turbines because a wake is generated between the front-row and back-row turbines, causing a wind speed deficit. Since wind power is proportional to the cube of wind speed, as shown in Eq. (1), substantial exploitable wind energy will be lost

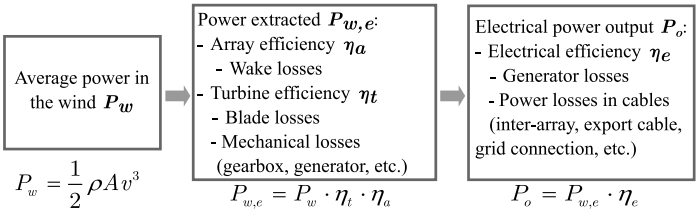

Fig. 3. Overall efficiency of a wind turbine including turbine, array, and electrical losses.

in the case of a significant deficit in wind speed due to close array spacing. Therefore, there should be enough space between the turbines to extract as much energy as possible from the incoming wind by reducing the wake power losses (Vermeer et al., 2003). Wake power losses can be alleviated by enabling wind speed recovery through the renewal of kinetic energy, particularly in the vertical direction for large arrays (Dupont et al., 2018). Besides choosing a farm layout with sufficient turbine spacing, wind farm flow control, which manipulates the wake between wind turbines, is investigated to increase the power output during operation (Kheirabadi and Nagamune, 2019).

The turbine and array losses is then be reflected on P_w such that the extracted power $P_{w,e}$ becomes:

$$P_{w,e} = \frac{1}{2}\ \rho\ A\ v^3\ \eta_t\ \eta_a\ , \tag{2}$$

where η_t and η_a stand for the turbine efficiency and array efficiency, respectively, as illustrated in Fig. 3. As mentioned above, modern large wind turbines offer maximum turbine efficiencies closer to 85% of the Betz limit, i.e., $\eta_{t_{max}} \approx 50\%$.

Lastly, as depicted in the rightmost category in Fig. 3, electrical losses incurred by the generator and the cable connections (inter-array and grid connections) should also be considered when calculating the electrical power output P_o. The number of wind turbines connected to the grid in a wind farm, array spacing, and location-specific parameters (distance to the grid connection point and coast, water depth, average wave height, etc.) determine the total length of inter-array cable connections/types and the total cable length for the grid connection, and hence, determine the total electrical losses. The power losses associated with transmission and distribution, i.e., after the grid connection point, are under the liabilities of the transmission and distribution system operators and, therefore, are not taken into account.

Given the significance of these parameters, a thorough analysis is required to estimate the energy yield, array efficiency, wake losses, and electrical losses for each site, which will be addressed in the next section.

3. Materials and methods

As highlighted in the Introduction, making investment decisions for large-scale projects, such as OWFs, poses a formidable challenge for companies and decision-makers. These investment decisions demand a multi-disciplinary analysis, encompassing various dimensions, including energy, politics, legislation, technology, economics, social impacts, and environmental issues. The overview of the demonstrated interdisciplinary framework is illustrated in Fig. 4.

Literature Review & Techno-economic Analysis: This initial phase delves into a comprehensive literature review, concentrating on the prevailing state-of-the-art knowledge surrounding offshore wind power studies and decision-making. Concurrently, we execute a detailed techno-economic evaluation, focusing specifically on power losses and an intricate power systems analysis for an alternative reactive power compensation model. It is pertinent to highlight that our research incorporates findings from this analysis for seven Norwegian offshore wind farm sites under investigation ($A_1 - A_7$). For clarity, the wind farm layout chosen, consisting of a grid layout with a 10 × 10 wind turbine configuration, serves as a generic model, enhancing the breadth and depth of our comprehensive analysis. It is worth noting that the projected installed capacities for these offshore site alternatives are subject to variation and may evolve in the future.

Decision-Making & Expert Surveying: Outcomes derived from the techno-economic analysis furnish vital inputs to our novel decision-making algorithm. This algorithm integrates 17 distinct decision-making criteria (C1 – C17). In order to ensure a holistic and expert-backed evaluation, we have engaged professionals from the field. These expert insights act as intermediaries, feeding into the decision-making algorithm and consequently assisting in generating a ranked list of the seven alternative wind farm sites.

Recommendations & Comparative Analysis: The concluding phase encapsulates an exhaustive comparative study, echoing both academic and industrial perspectives. This not only provides a meticulous comparison but also offers recommendations spanning technical, economic, and energy policy facets, offering a forward-looking outlook.

Prior to delving into the descriptions of the seven alternative locations, the selected criteria for this study are introduced in the subsequent section.

3.1. Identification of decision-making criteria

In this section, the definitions of the influencing criteria are explained. The subject-associated criteria definitions are investigated under two main groups: (1) techno-economic and (2) environmental and social incorporating, legislative focus & opinion. The hierarchical structure of OWF site selection is shown in Fig. 5.

C1: Mean wind speed

Mean wind speed is a crucial technical criterion in determining the most suitable location for a wind power project. Pressure differences in the atmosphere are what create wind flow, which is essentially kinetic energy. Wind power is generated from this kinetic energy and is directly proportional to the cube of the wind speed (see Section 2.2).

C2: Net Annual Energy Yield (AEY)

Annual energy yield (AEY) is an indication of the amount of electrical energy that can be generated by a wind turbine, wind farm, or a larger area over the course of a year. The net AEY is determined by taking into account the factors discussed in the preceding section and other factors such as the efficiency of the power system components, the length and type of cable, the wind farm's location, and the wind turbine layout. The net AEY can be quantified in the form of kilowatt-hours (kWh), megawatt-hours (MWh), or gigawatt-hours (GWh).

C3: Net Capacity Factor (CF)

The net CF is the ratio between the actual or estimated net AEY of a wind farm or turbine and the maximum energy production achievable if the system were to be run for the whole year (8760 h).

C4: Average water depth

The average water depth of a potential site is a significant factor for the successful deployment of floating offshore wind turbines, as the turbines must be securely moored to the seabed to avoid drifting where the length of the mooring lines is determined by the water depth.

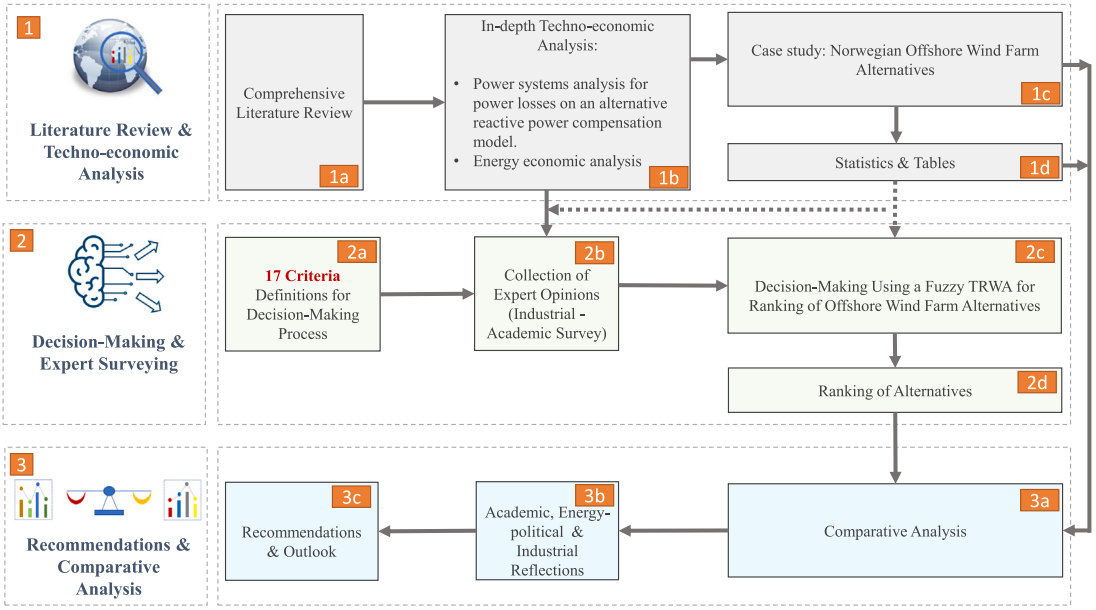

Fig. 4. Process of integrating OWF Energy specific case-study and MCDM framework.

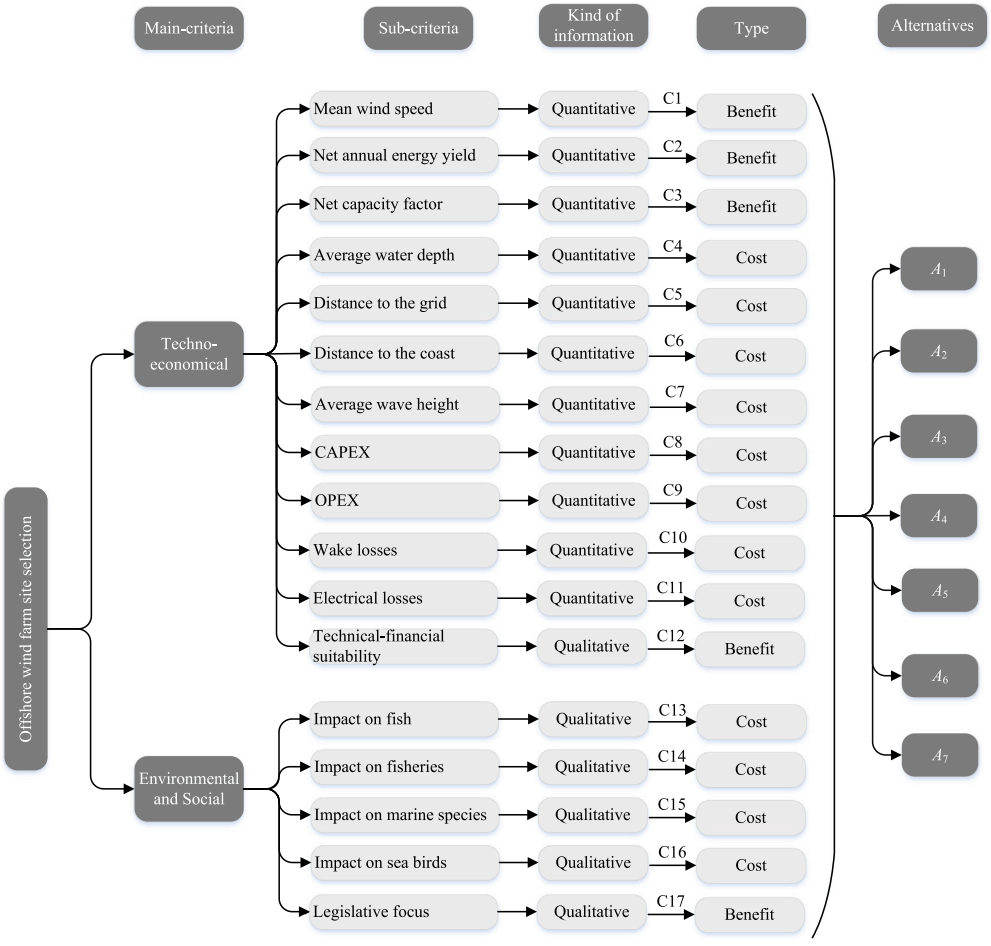

Fig. 5. The decision hierarchy of the OWF site selection problem. C1–C17 stand for criteria, and A_1–A_7 stands for alternative OWF sites.

C5: Distance to the nearest grid connection point

The proximity of the nearest power grid transformer or substation is a major factor influencing both technical and economic aspects, such as power losses associated with the type, length, and power system topology of the planned OWF and capital expenditures (CAPEX) related to the electrical works, respectively. Therefore, the closest existing transformer station onshore is used if it has the capacity to accommodate additional power from the potential new OWF.

C6: Distance to coast

Construction, operation, and decommissioning are all significantly affected by proximity to the shore. The time it takes to transport the vessel for repair adds up to a hefty sum throughout the course of its working life. However, specifics like the locations of viable harbours were neglected for the sake of this investigation.

C7: Average wave height

The average wave height is noteworthy due to the OWF's accessibility for maintenance ships. The transportation of wind turbines, the specifications of the mooring system, the development and tuning of offsetting control systems and other related components are all impacted by the wave conditions.

C8: CAPEX

Expenditures made on capital equipment and structures at the outset of an operation to produce an OWF are referred to as CAPEX. Some examples of OWF-specific CAPEX include the cost of wind turbines and their associated components, such as foundations, electrical works, civil works, project development, and permits.

C9: OPEX

OPEX refers to operational expenditures, which are the OWF's running expenses. OWF-specific OPEX numbers include the cost of operation and maintenance, spare parts, employee wages, insurance, overheads, and other related expenditures.

C10: Wake losses

The extraction of energy from the wind by wind turbines results in the reduction of wind speed downstream of the turbines, creating a wake. This wake spreads as it proceeds downstream and eventually recovers towards free-stream conditions. The combined impact of the changes in wind speed resulting from the interaction of wind turbines with each other is referred to as the wake effect or wake loss, which can significantly impact the energy production of a wind farm. Therefore, it is crucial to take into account the wake losses from adjacent wind farms as well as the potential impact of future wind farms.

C11: Electrical losses

Electrical losses in the inter-array cable system are one of the most important criteria for offshore wind projects. The greater the distance between turbines, the greater the inter-array cabling losses. Export cable losses refer to the energy lost during the transmission of power from an offshore wind farm to the onshore grid. The export cable losses increase with the distance between the offshore wind farm and the onshore grid. It is crucial for the economic sustainability of offshore wind projects to minimise these losses. By minimising electrical losses, more energy may be provided to the grid, increasing the profitability of the project and lowering the price of power for customers.

C12: Technical-financial suitability

The areas under consideration are assessed with regard to their attractiveness from an economic and technological perspective. Issues related to whether technological development or good production conditions at sea can justify the extra cost of going offshore are important when determining where offshore wind power should be built in Norway (Berg et al., 2012).

C13: Impact on fish

The influence on fish is also a qualitative indicator that assesses the wind farm's potential environmental impact on specific fish species (Berg et al., 2012). The maximum reported effect is utilised if the wind farm region coincides with the spawning, reproduction, and feeding areas of many fish species that would be impacted.

C14: Impact on fisheries

The effect on fisheries used here is based on the Norwegian Directorate of Fisheries' estimate, which takes three elements into account: (i) the primary sales value, (ii) the number of boats under 15 m, and (iii) an expert appraisal of the overall value for fisheries. The total of these parameters is used to calculate the effect on fisheries (Langeland and Veim, 2012).

C15: Impact on marine species

Marine species are vulnerable to the impacts of offshore wind farms. The construction noise, for instance, can affect their ability to communicate, navigate, and detect prey. Additionally, the turbines and their supporting structures can cause habitat loss and reduce the quality of feeding and breeding areas for marine species. To minimise the impact of offshore wind farms on marine species, various mitigation measures can be taken. These measures include selecting appropriate turbine locations within the investigation areas, reducing the operation noise and vibration, and using advanced detection and monitoring systems. However, it is crucial to note that each species has its unique needs and sensitivities, and mitigation measures need to be tailored accordingly.

C16: Impact on sea birds

The impact on sea birds is a measure that indicates the qualitative impact on sea birds caused by commissioning, operation, decommissioning, area utilisation, bird migration, barrier impacts, and oil spill (Berg et al., 2012).

C17: Legislative focus

A qualitative factor that assesses the stance towards offshore wind generation is the consideration of high-level legislative focus or political support. Legislative focus influences various aspects, such as the process of awarding a new OWF concession, the integration of wind power into the national electrical grid, and planned involvement in wholesale electricity markets.

The subsequent section describes seven Norwegian OWF sites, presenting them as alternative locations for OWFs and detailing their suitability for either bottom-fixed or floating foundation types.

3.2. Alternative locations for offshore wind farms in Norway

The Norwegian Water Resources and Energy Directorate (NVE) identified potential sites for offshore wind in 2010 (Drivenes et al., 2010), as shown in Fig. 6, incorporating sites relevant for both floating and bottom-fixed wind farms. NVE recommends that the areas that are to be opened should be well-suited for wind power production and attractive to potential developers and that technical and economic factors should be the main criteria when prioritising areas (Berg et al., 2012).

NVE has categorised the investigation areas into three categories: A, B, and C, as shown in Fig. 6 and Table 1. Category A includes investigation areas that are well-suited from a technical and economic standpoint and have relatively few conflicting interests. Category B includes investigation areas that have some challenges related to technical aspects and/or existing land interests or natural environment, but these challenges can be solved by future technological development, grid measures, and/or mitigating measures. Category C includes investigation areas that have significant land conflicts that are not easily solvable by mitigating or consequence-reducing measures, but these conflicts are not so significant that opening the areas is impossible. The sites for each category are listed in Table 1.

Two sites are chosen from each category to be studied in this work, with the exception of Category A. The selected offshore sites are highlighted in magenta in Fig. 6 and are italicised in Table 1. NVE assumed that Sørlige Nordsjø I and Sørlige Nordsjø II would be mutually exclusive areas but did not find any basis for prioritising one over the other with existing knowledge in 2012 (Berg et al., 2012). In

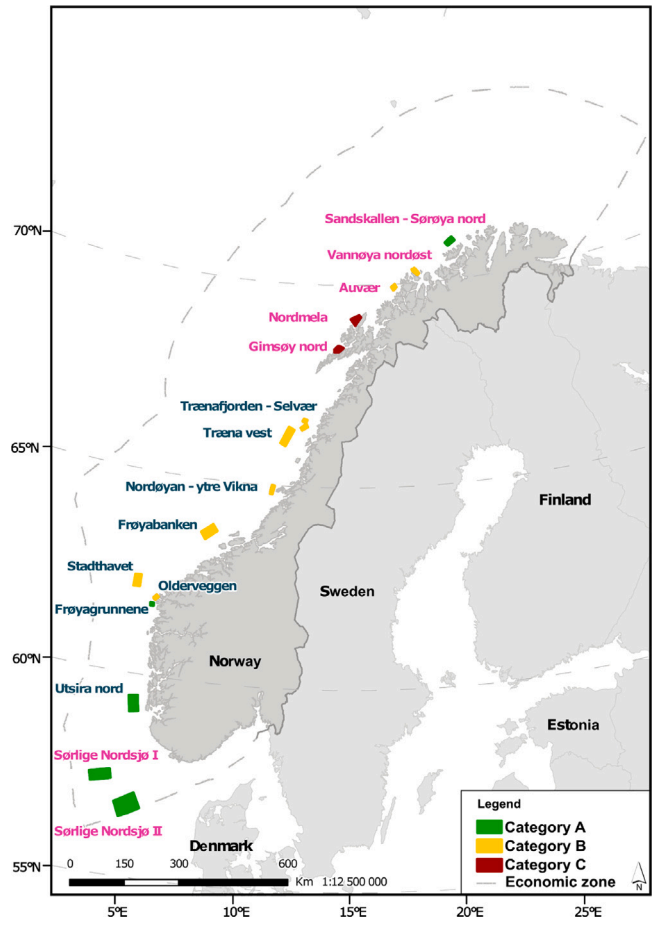

Fig. 6. Map showing the alternative locations of offshore wind farm sites in Norway, including the seven selected sites shown in *magenta*.

addition, Norwegian TSO Statnett assessed that only one of the areas could be connected to the Norwegian grid by 2025 (NVE, 2017). On 12th June 2020, the government decided to open Utsira Nord and Sørlige Nordsjø II for offshore renewable energy production and that the power from the first phase of Sørlige Nordsjø II (1500 MW) will be sent to the Norwegian mainland (Ministry of Petroleum and Energy, 2021). The announcement of the first phase of Sørlige Nordsjø II and Utsira Nord is planned for the first quarter of 2023, with a subsequent allocation of the areas during the year. NVE thought these areas stood out as areas with excellent technical-economic conditions, and those overall consequences were assessed as acceptable. Furthermore, NVE recommended that Gimsøy Nord and Nordmela should not be prioritised to be opened for wind power development in the first instance out of consideration for the overall consequences for land use and environmental interests (category C). However, other areas might be opened based on the assessment by NVE. The development of offshore wind farms in these areas (category B) will occur at a later stage, contingent upon advancements in technology, availability of internet access, and a favourable balance of interests.

The ranking to be provided in this work will cast more light on these mutually exclusive areas and be compared with the government's decision over the Sørlige Nordsjø sites. Most of the chosen sites are reported as suitable for a mix of bottom-fixed and floating wind turbines (Drivenes et al., 2010). More detailed information for the chosen sites is given in the following section, which is retrieved from the reports by NVE, Multiconsult and the government (Berg et al., 2012; NVE, 2017; Drivenes et al., 2010; Multiconsult, 2012; Ministry of Petroleum and Energy, 2021; Statnett, 2021, 2022).

Table 1
NVE's categorisation of survey areas for wind power development with respect to recommended opening priorities (Berg et al., 2012; NVE, 2017). Italic text showcases the chosen sites in this work.

Category A	Category B	Category C
Sandskallen-Sørøya Nord	*Vannøya Nordøst*	*Nordmela*
Sørlige Nordsjø I & II	*Auvær*	*Gimsøy Nord*
Utsira Nord	Trænafjorden - Selvær	
Frøyagrunnene	Træna vest	
	Nordøyan - Ytre Vikna	
	Frøyabanken	
	Stadthavet	
	Olderveggen	

3.2.1. A_1 – Sørlige Nordsjø I offshore wind farm

Sørlige Nordsjø I lies approximately 150 km from the coast (Fig. 7) and is in relative proximity to planned interconnections between Norway and Germany, Norway and the Netherlands, and Norway and the United Kingdom.

The wind conditions are estimated to permit a capacity of 1000–1500 MW, and the area has a total size of 1375 km^2, the second largest area after Sørlige Nordsjø II. Both bottom-fixed and floating foundation technologies may be applicable as large parts of the region have sea depths between 50 and 70 m. The area is located approximately 200 km from the nearest land connection point, and the most relevant connection points are Feda or Lista (Berg et al., 2012). NVE is considering two connections between Norway and Germany, both planned with a transmission capacity of 1400 MW and connection points near Tonstad in Sirdal municipality, as of September 2010 (Drivenes et al., 2010). If a potential wind power plant is to be connected to land with its own cable, it would be beneficial to do so at already established connection points for international cables in Vest-Agder, more specifically Feda or the area around Tonstad. This is because the wind power from the Sørlige Nordsjø I is likely to be exported to foreign countries for much of the time. Such a solution could still require reinforcement of the land grid, especially in order to handle situations where there is a significant amount of production from the wind power plant at the same time as there is import to Norway. A third solution for connecting a wind power plant in this area could be to connect it directly to a foreign country, such as Germany, without a connection to Norway (Drivenes et al., 2010).

The wind conditions of the Sørlige Nordsjø I site are described in the wind rose in Fig. 8. The mean wind speed of the site is 10.60 m/s, which is the highest of all sites considered in this work. Wind directions vary greatly for all wind speeds, with only a sector in the northeast (approximately 120 degrees) showing relatively low wind frequencies. The high mean wind speed means that the wind speed is only below the turbine cut-in speed for approximately 10–11% of the time; however, it is above the cut-out speed for about 0.7–0.8% of the time.

3.2.2. A_2 – Sørlige Nordsjø II offshore wind farm

Sørlige Nordsjø II lies approximately 140 km from the coast (Fig. 9) and is in relative proximity to planned interconnections between Norway and Germany, Norway and the Netherlands, and Norway and the United Kingdom. The wind conditions are estimated to permit a capacity of 1000–2000 MW, and the area has a total size of 2591 km^2, the largest area among the others studied here. Similar to Sørlige Nordsjø I, both bottom-fixed and floating foundation technologies may be applicable as large parts of the area have sea depths between 60 and 70 m. The area is located approximately 200 km from the nearest land connection point, and the most relevant connection points are Feda or Lista (Berg et al., 2012).

Sørlige Nordsjø I and II are mutually exclusive areas. Norwegian TSO Statnett further assessed that it may be possible to realise development in both areas in the long run. This, however, assumed that at least one of the areas would either be connected to an exchange

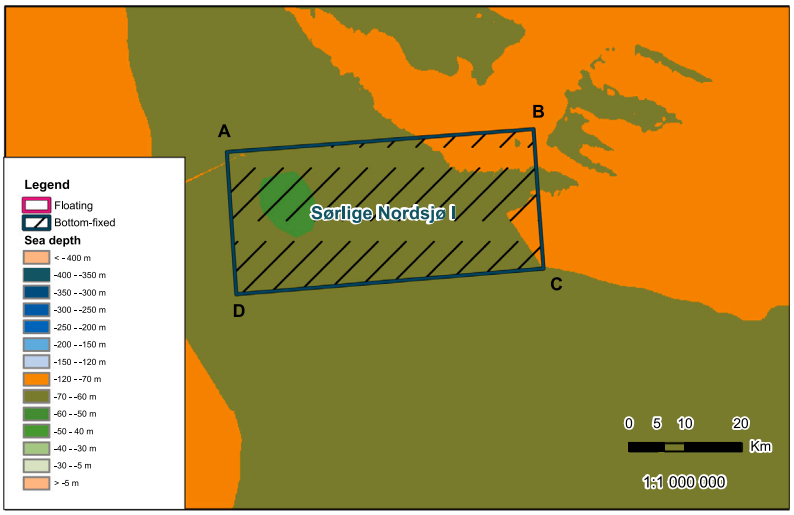

Coordinates:

A	3° 02′ 43″ E	57° 28′ 13″ N
B	3° 55′ 37″ E	57° 35′ 18″ N
C	4° 01′ 21″ E	57° 22′ 21″ N
D	3° 08′ 42″ E	57° 15′ 03″ N

Fig. 7. Sea depths at Sørlige Nordsjø I site with coordinates.
Source: Adapted from Berg et al. (2012).

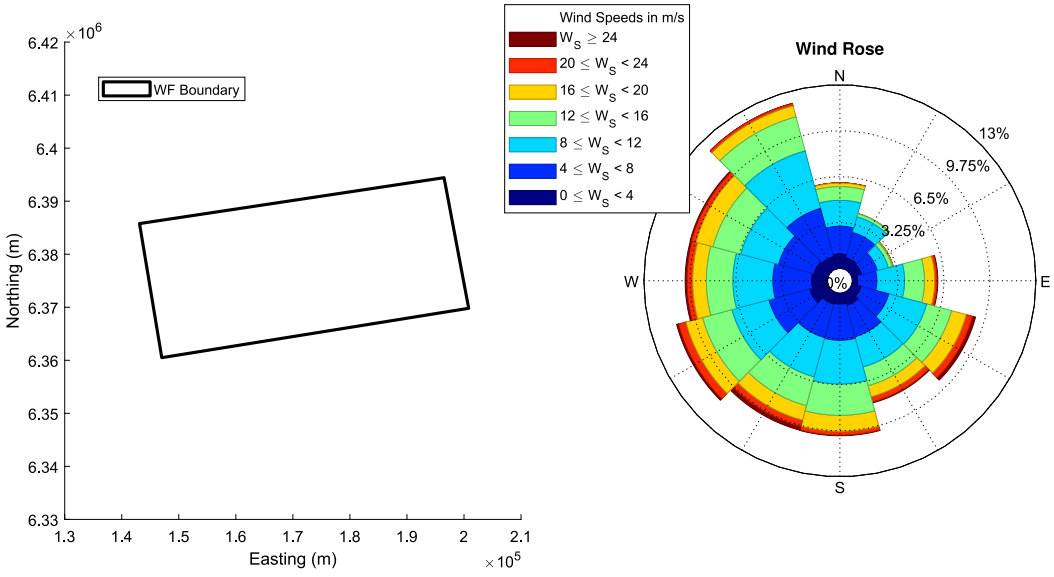

Fig. 8. Wind farm boundary coordinates and wind conditions of the Sørlige Nordsjø I site.

cable or directly to Continental Europe/Great Britain without a network connection to Norway (NVE, 2017). A recent report from Statnett (2022) implies that both Southern Norway and Eastern Norway (Greenland) are real alternatives for the connection of offshore wind from the Sørlige Nordsjø II in phase 2. In later phases, it is intended to be connected to the countries around the Nordsjø (led by Germany, the Netherlands, Denmark and Belgium) (Statnett, 2022).

The mean wind speed of the Sørlige Nordsjø II site is the second highest of all seven sites considered, at 10.58 m/s, second only to the Sørlige Nordsjø I site. The wind rose for Sørlige Nordsjø II, Fig. 10, is slightly less uniform than the Sørlige Nordsjø I site, with the majority of wind directions coming from the eastern half of the wind rose. The highest wind speeds are more evenly distributed, with some coming also from a south-easterly direction. The high mean wind speed for this site means that only 9–10% of wind speeds are below cut-in and 0.6–0.7% are above cut-out.

3.2.3. A_3–Gimsøy Nord offshore wind farm

Gimsøy Nord is located northwest of Gimsøy in Vågan Municipality, Nordland County (Fig. 11). The wind conditions are estimated to permit a capacity of 100–300 MW, and the area has a total size of 245 km^2. A large proportion of the study area has depths between 20 and 40 m. Therefore, only bottom-fixed foundation technology is considered suitable for this area. It has been assessed that a network connection can be carried out without significant challenges and without the need for larger reinforcements of existing networks (Berg et al., 2012). Gimsøy Nord is close to land, and development in the area will be clearly visible from several areas where landscape and outdoor values are considered nationally important.

The wind conditions for the Gimsøy Nord site are described in the wind rose in Fig. 12. The mean wind speed of the site is 8.45 m/s, with the wind predominantly coming from a southerly direction. The highest wind speeds are seen in a direction from the southwest. Wind speeds below cut-in account for approximately 16–17% of wind conditions, with wind speeds above cut-out accounting for approximately 0.2–0.3% of wind conditions.

3.2.4. A_4–Nordmela offshore wind farm

Nordmela is located close to Andøya in the Andøy Municipality, Nordland County (Fig. 13). The wind conditions are estimated to permit

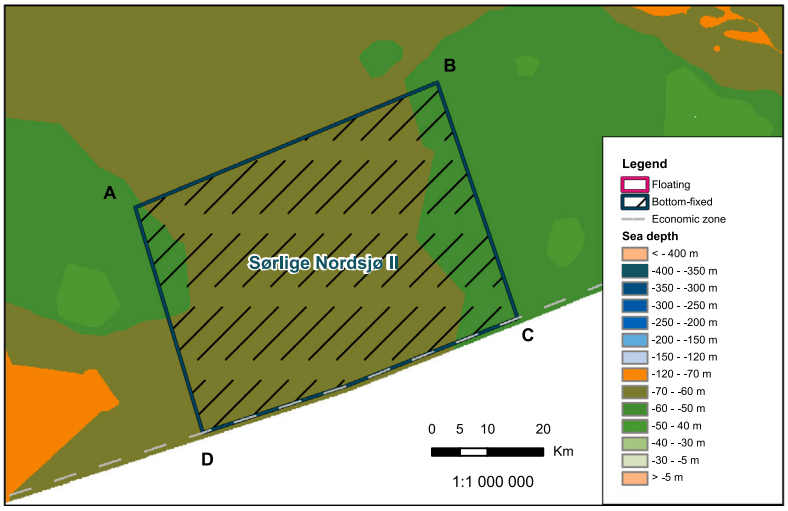

Coordinates:

A	4° 20′ 48″ E	56° 49′ 24″ N
B	5° 10′ 05″ E	57° 05′ 36″ N
C	5° 29′ 51″ E	56° 44′ 17″ N
D	4° 38′ 29″ E	56° 29′ 02″ N

Fig. 9. Sea depths at Sørlige Nordsjø II site with coordinates.
Source: Adapted from Berg et al. (2012).

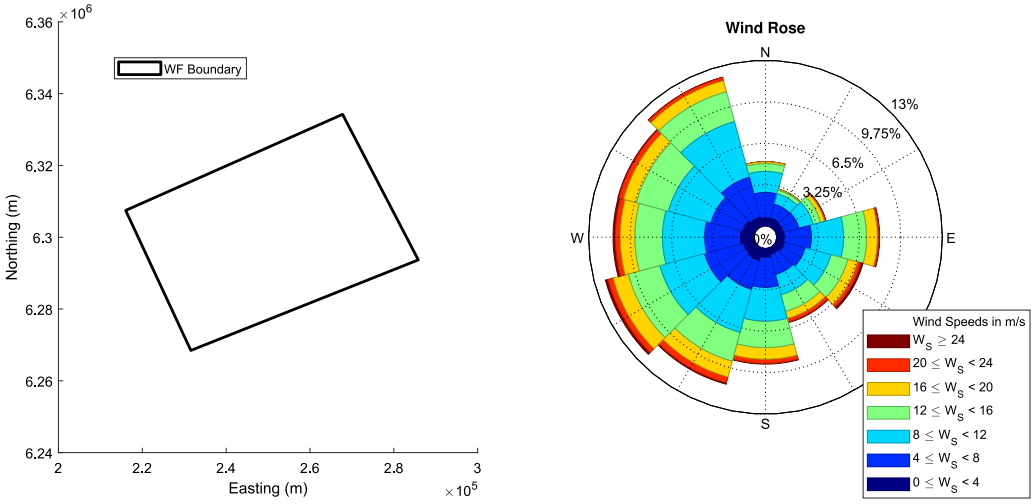

Fig. 10. Wind farm boundary coordinates and wind conditions of the Sørlige Nordsjø II site.

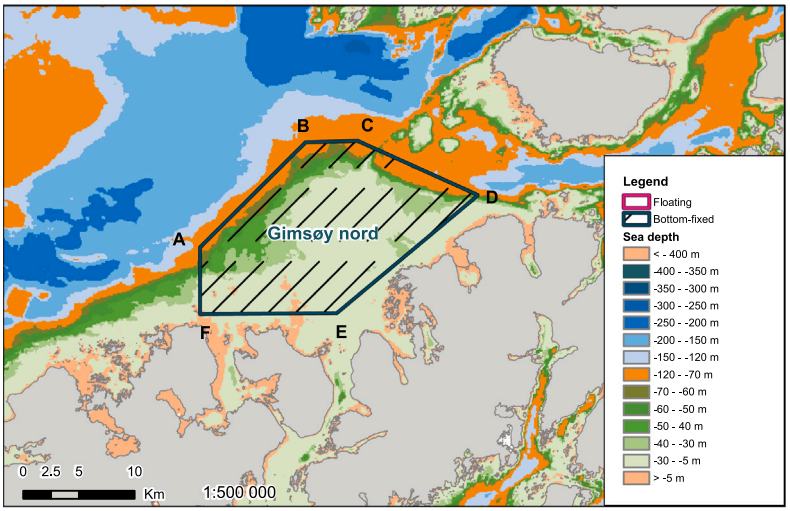

Coordinates:

A	13° 58′ 45″ E	68° 24′ 30″ N
B	14° 12′ 23″ E	68° 29′ 38″ N
C	14° 19′ 13″ E	68° 29′ 44″ N
D	14° 34′ 57″ E	68° 27′ 11″ N
E	14° 16′ 43″ E	68° 21′ 25″ N
F	13° 58′ 54″ E	68° 21′ 18″ N

Fig. 11. Sea depths at Gimsøy Nord site with coordinates.
Source: Adapted from Berg et al. (2012).

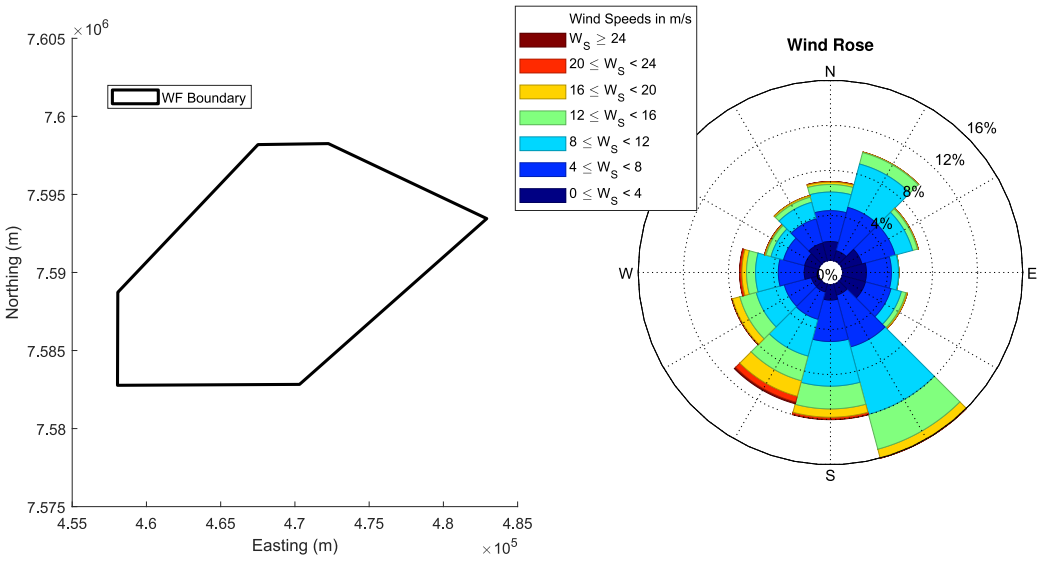

Fig. 12. Wind farm boundary coordinates and wind conditions of the Gimsoy Nord site.

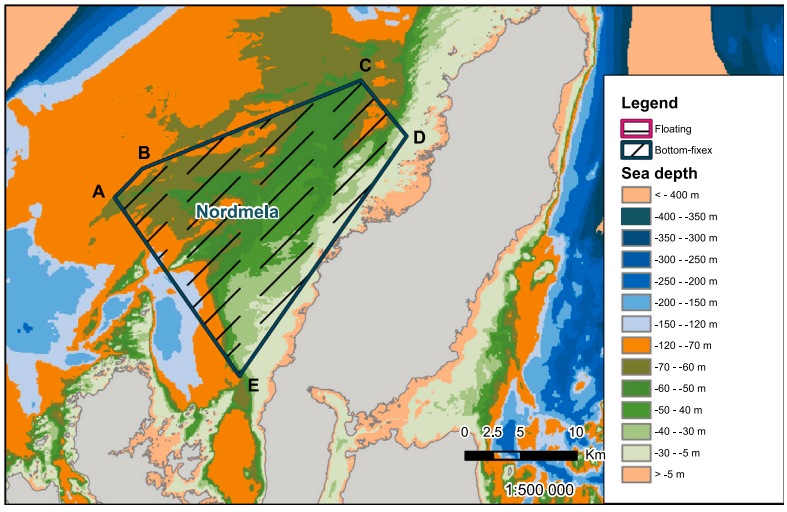

Coordinates:

A	15° 06′ 22″ E	69° 09′ 31″ N
B	15° 10′ 10″ E	69° 10′ 54″ N
C	15° 39′ 50″ E	69° 15′ 06″ N
D	15° 45′ 58″ E	69° 12′ 22″ N
E	15° 23′ 21″ E	69° 01′ 01″ N

Fig. 13. Sea depths at Nordmela site with coordinates.
Source: Adapted from Berg et al. (2012).

a capacity of 100–300 MW, and the area has a total size of 332 km^2. The majority of the investigation area has sea depths between 20 and 80 m, and it is assumed that both fixed and floating foundation technologies may be suitable. The network connection will require significant network investments and is likely to be possible only after 2025 (Berg et al., 2012). Any construction on the site will be well visible from Andøya and several culturally important areas of high value.

The wind direction for the Nordmela site is largely consistent, with the wind coming from the south or northeast. The wind rose in Fig. 14 shows this distribution of wind direction as well as information on the wind speed. The highest wind speeds are typically experienced when the wind direction is from the south, and the mean wind speed for the site is 8.19 m/s. For approximately 14–15% of the year, the wind speed drops below that of the turbine cut-in speed and for 0.2–0.3% of the year, it is above the cut-out speed.

3.2.5. A_5–*Auvær offshore wind farm*

Auvær is located in the Barents Sea, approximately 15 km off of Kvaløya in TromsøMunicipality, Troms County (Fig. 15). The wind conditions are estimated to permit a capacity of 100–300 MW, and the area has a total size of 105 km^2. A large portion of the area has depths between 20 and 40 m, and only bottom-fixed foundation technologies are assumed to be feasible. The network connection of a wind turbine in this area will require significant investments in underlying networks (Berg et al., 2012).

The wind rose in Fig. 16 describes the wind conditions for the Auvær site. The predominant wind direction is from the south-westerly quadrant with a smaller, yet significant, peak showing wind directions from the northeast. The mean wind speed for the site is 8.13 m/s, and for 17–18% of the year, the wind speed is below the cut-in speed, while it is above the cut-out speed for approximately 0.2–0.3% of the year.

3.2.6. A_6–*Vannøya Nordøst offshore wind farm*

The investigation area Vannøya Nordøst is located in the Barents Sea, close to Vannøya in the Karlsøy municipality, Troms county (Fig. 17). The area has a total size of 154 km^2. The majority of this site has sea depths between 20 and 80 m, and it is assumed that both fixed and floating foundation technologies could be viable. The wind conditions are estimated to permit a capacity of 100–300 MW. The grid connection of a wind farm in the area will require substantial

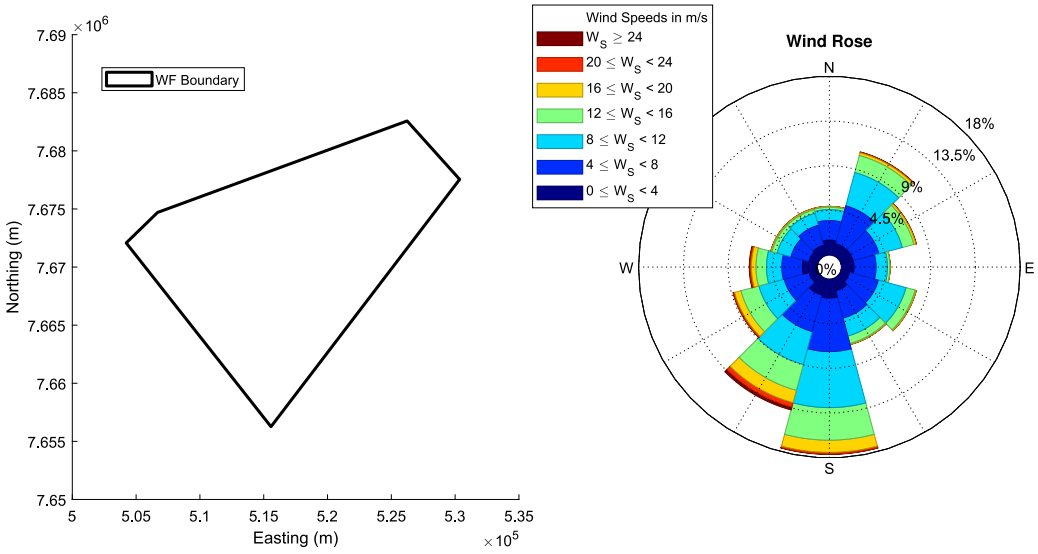

Fig. 14. Wind farm boundary coordinates and wind conditions of the Nordmela site.

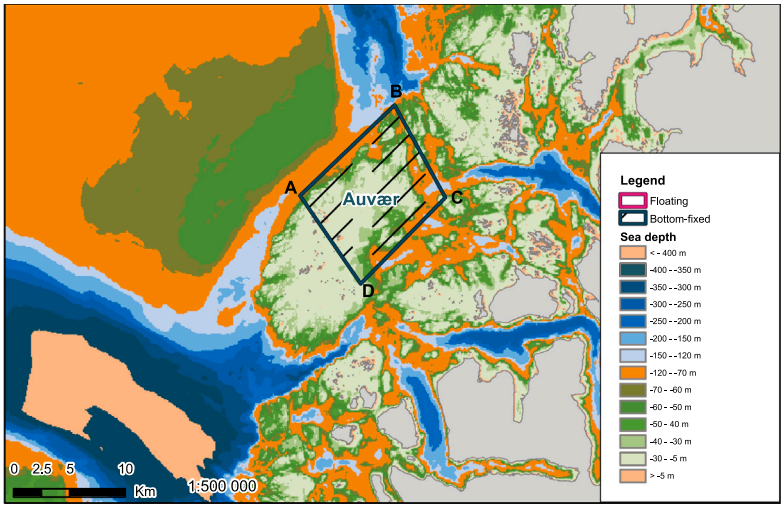

Coordinates:

A	18° 00′ 25″ E	69° 55′ 52″ N
B	18° 14′ 23″ E	69° 59′ 60″ N
C	18° 20′ 49″ E	69° 55′ 24″ N
D	18° 08′ 18″ E	69° 51′ 27″ N

Fig. 15. Sea depths at Auvær site with coordinates.
Source: Adapted from Berg et al. (2012).

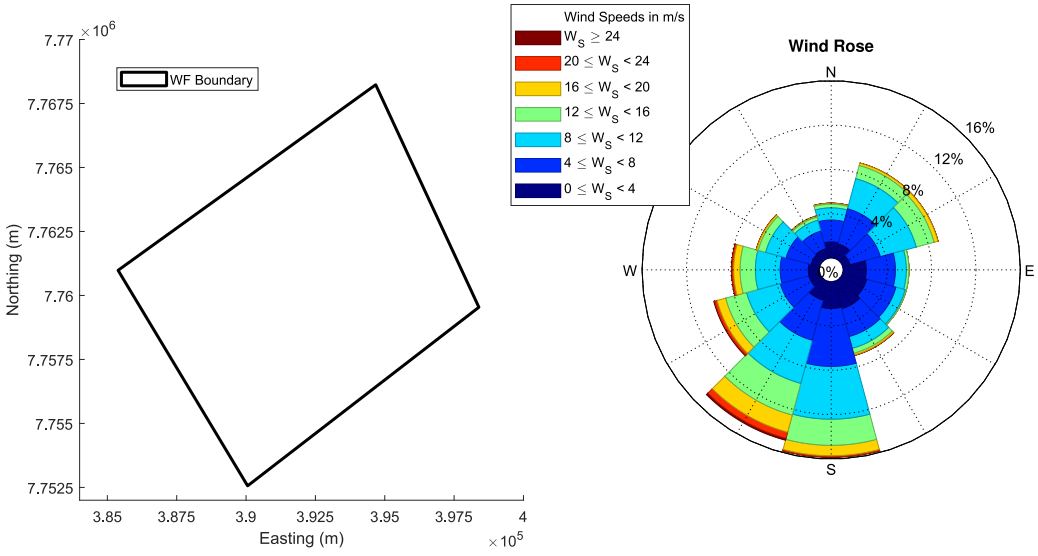

Fig. 16. Wind farm boundary coordinates and wind conditions of the Auvær site.

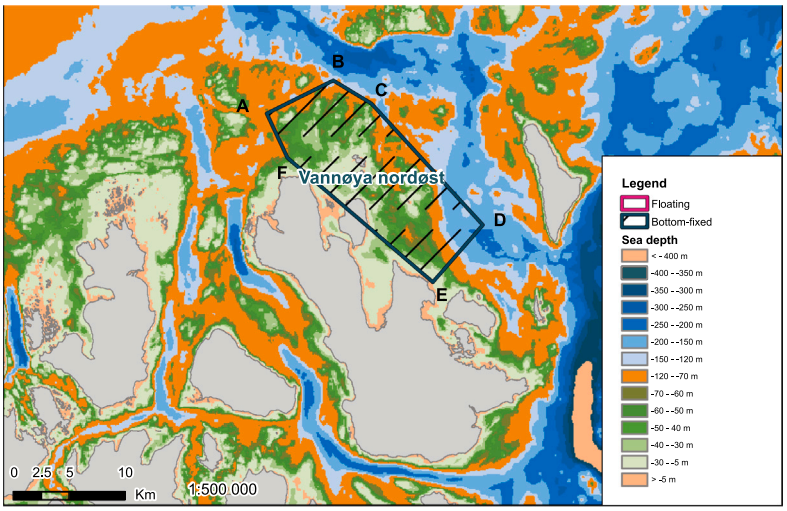

Coordinates:

A	19° 33′ 38″ E	70° 20′ 12″ N
B	19° 43′ 31″ E	70° 21′ 32″ N
C	19° 48′ 42″ E	70° 20′ 17″ N
D	20° 03′ 09″ E	70° 14′ 01″ N
E	19° 55′ 25″ E	70° 11′ 28″ N
F	19° 36′ 06″ E	70° 17′ 59″ N

Fig. 17. Sea depths at Vannøya Nordøst site with coordinates.
Source: Adapted from Berg et al. (2012).

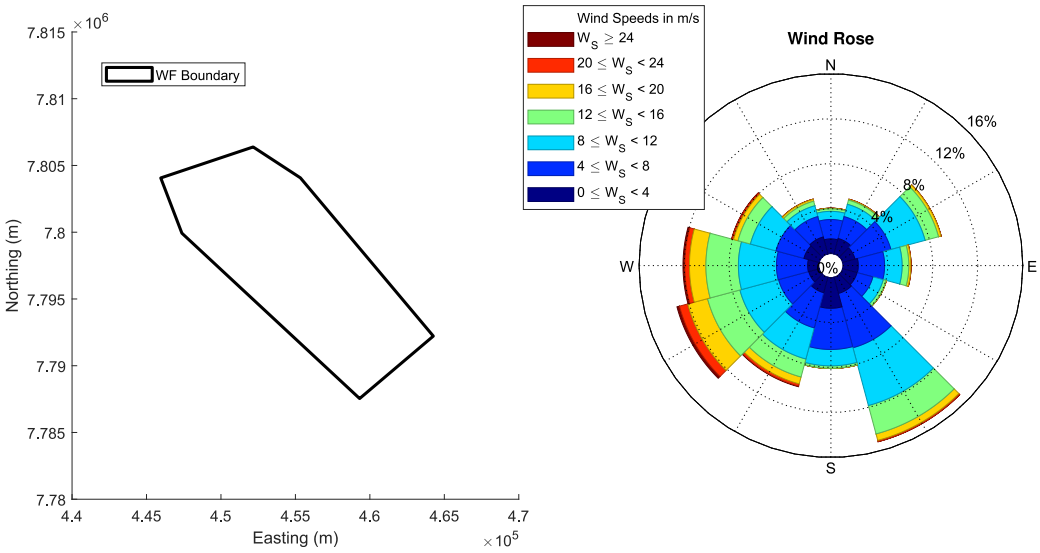

Fig. 18. Wind farm boundary coordinates and wind conditions of the Vannøya Nordøst site.

investments in underlying networks and is likely to be possible only after 2025 (Berg et al., 2012).

The wind conditions at the Vannøya Nordøst site can be seen in Fig. 18 with the wind rose describing annual wind speed, direction, and frequency. The wind direction at the site is mostly from the west or southeast, although around 9–10% of the time from the northeast. Wind direction is more consistent than some of the other sites in this study, with wind directions from the north or east-south-east rarely experienced. The mean wind speed for the site is 7.93 m/s, falling below the cut-in speed around 17–18% of the year and above the cut-out around 0.3–0.4% of the year. The highest wind speeds are typically from the west.

3.2.7. A_7–Sandskallen-Sørøya Nord offshore wind farm

Sandskallen-Sørøya Nord is located in the Barents Sea, about 14 km off the coast of Sørøya in Hammerfest Municipality in Finnmark County (Fig. 19). The area has a total size of 260 km^2. Most of the area lies in depths between 40 and 80 m, and the area is suitable for both floating and bottom-fixed foundation technologies.

The wind conditions permit a capacity of 100–300 MW. The area is located in a region where increased load uptake is expected, and a wind farm in the area can be connected to the central grid without incurring major costs in the underlying network. To strengthen the security of supply to Northern Norway and to link to a larger amount of new production, Norwegian TSO Statnett has applied to NVE to build two new 420 kV connections (Berg et al., 2012).

The annual wind conditions of the Sandskallen-Sørøya Nord site can be seen summarised in the wind rose in Fig. 20. The mean wind speed is 8.82 m/s, with the predominant wind direction being from the south-west. However, it can be seen in the wind rose that the wind direction is quite variable, resulting in a relatively evenly distributed wind rose when compared to other sites. The wind speed, for all directions, falls under typical cut-in speeds of turbines (4 m/s) approximately 14–15% of the year and above the cut-out speed (25 m/s) approximately 0.1–0.2% of the year. The highest wind speeds, above-rated wind speeds, typically come from the west or south.

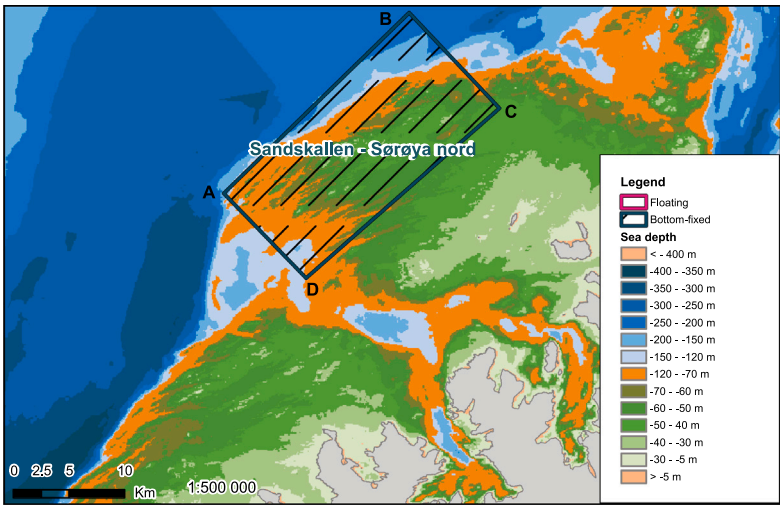

Coordinates:

A	22° 12′ 01″ E	70° 55′ 10″ N
B	22° 42′ 35″ E	71° 02′ 44″ N
C	22° 54′ 03″ E	70° 57′ 36″ N
D	22° 22′ 34″ E	70° 50′ 37″ N

Fig. 19. Sea depths at Sandskallen-Sørøya Nord site with coordinates.
Source: Adapted from Berg et al. (2012).

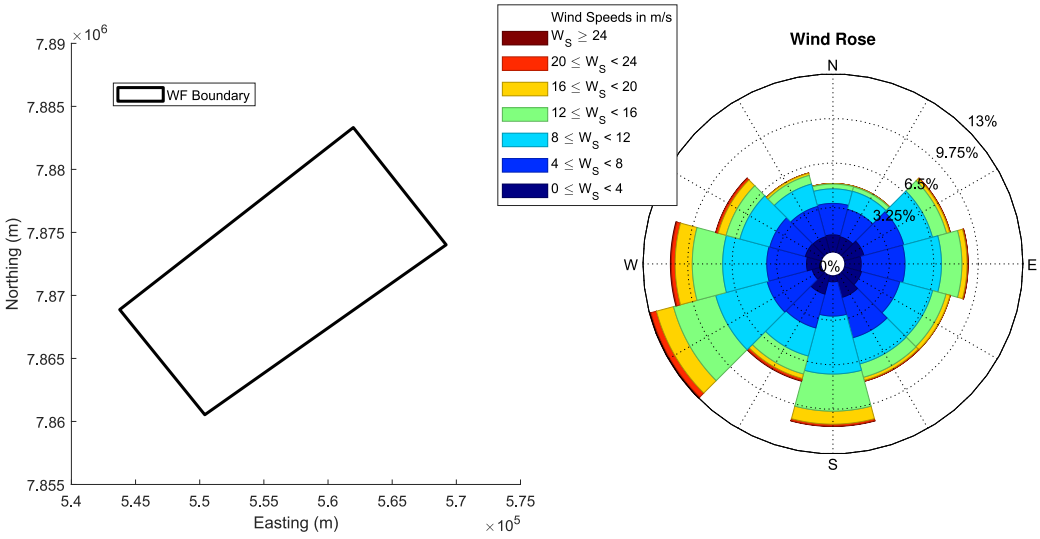

Fig. 20. Wind farm boundary coordinates and wind conditions of the Sandskallen-Sørøya Nord site.

3.3. Wind power output calculations

3.3.1. Mean wind speed, net annual energy yield and net capacity factor calculations

A mix of data sources is required to determine the gross AEY of the selected offshore wind farm locations. Firstly, we utilised the Renewables.ninja tool (Staffell and Pfenninger, 2016), a website based on the The Modern-Era Retrospective Analysis for Research and Applications Version 2 (MERRA-2) dataset provided by NASA's Global Model and Assimilation Office (GMAO) (Global Modeling and Assimilation Office, 2023), to simulate the wind speed at a chosen coordinate and year using historical data and a selected turbine model (capacity and hub height). The simulated results, including local date and time, power output, and wind speed, were exported with a one-hour resolution. Data in Renewables.ninja was only provided for 2019, thus limiting the data to one year. Otherwise, the average of the available data would be used.

We utilised the wind farm model presented in Taylor et al. (2021) to determine the gross AEY of each site, employing wind speed data from Renewables.ninja and wind direction from the Global Wind Atlas (DTU, 2023). These data sources collectively provided a wind rose, as presented for each site in the previous section. Subsequently, we ran the wind farm model using the wind rose with a single turbine, ensuring that no wake losses were considered in the gross AEY calculation.

The net AEY was determined by subtracting the electrical and wake losses from the gross AEY. The mean wind speed value for each site was computed by calculating the mean value of the wind speed data, provided in one-hour resolution increments, over the entire year. Furthermore, the net CF was calculated by dividing the net AEY by the maximum energy production achievable throughout the entire year. Details regarding the turbines and losses are provided below.

3.3.2. Turbines, array efficiency and wake losses

Each site has the same type of turbines, array spacing, and layout, as shown in Fig. 21. The chosen turbine is the Vestas V164 9500, which has a rated power of 9.5 MW, a rotor diameter of 164 m, and a hub height of 104 m. The power curve used for the turbine was taken from Pandit and Kolios (2020), and the thrust curve was assumed to be the same as that presented in Baptista et al. (2021) for the Vestas V164 8000 turbine. A regular rectangular grid of 100 turbines was used for each site, with the same row and column spacing used across all sites. The row and column spacing was set to be equal to 9 D and 6 D, respectively (1476 m and 984 m), where D is the rotor diameter, in line with reasonable assumptions laid out in Borrmann

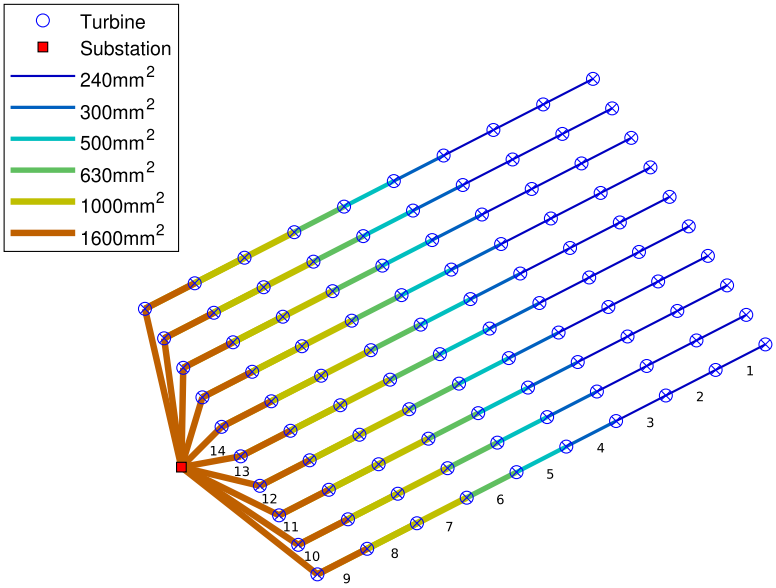

Fig. 21. Array cable layout including cable conductor sizes used for each of the seven sites. Numbers (1–14) designate the cable sections/positions in Table 3.

Table 2
Properties of the turbine and array.

Parameter	Value
Turbine model	Vestas V164 9500
Turbine capacity	9.5 MW
Rotor diameter (D)	164 m
Array size	10 × 10
Total capacity	950 MW
Turbine spacing (r, c)	$9D, 6D$
Hub height	104 m

et al. (2018). The angle of the columns of turbines was aligned with the predominant wind direction for each site (shown by the wind roses in Section 3.2), such that the larger spacing (row spacing) was in line with the predominant wind direction. Zhang et al. (2022) recommends a tandem configuration with a 9.25 D distance for wind farm design. This value is very close to the configuration selected for this study. The properties of the turbine and array are tabulated in Table 2.

In order to determine the array efficiency and wake losses for each site, the gross AEY values were used. The wind farm model used to determine the annual energy yield and wake losses of each site was presented in Taylor et al. (2021). The model uses the Larsen wake model, a rotor-effective wind speed calculation, and an energy conservation (root-sum-square) method for the summation of multiple wake effects to model the wake losses of the turbines in the farm.

3.3.3. Power calculation and electrical losses

The electrical layout of each of the seven sites is arranged into ten strings of ten turbines, as can be seen in Fig. 21. Six different cable sizes are used within the cable network, with conductor cross-sectional areas between 240 mm^2 and 1600 mm^2. Key parameters of the cable set used are provided in Table 3. Additional parameters, which are the same across all cable sizes, include a temperature coefficient of resistance of 0.00393 K^{-1}, a thermal resistivity of insulation of 3.5 K m/W, an insulation thickness of 9 mm, an insulation loss factor of 0.001, a maximum operating temperature of 90 °C, and an array voltage of 66 kV.

A Weibull distribution for each site was extracted from the wind speed data, as mentioned previously, and with the turbine power curve, a current profile for each cable section can be calculated. A reactive power component is considered by using a non-unity power factor, and the Joule losses, charging current losses, and dielectric losses are all considered in the final electrical loss value for each cable connection. These losses are calculated in line with the British Standards for electrical cables and the calculation of current rating (IEC, 2012). It is worth noting that this standard considers four thermal resistances to calculate temperature increase in buried cables, which are: T_1 between conductor and sheath, T_2 between sheath and armour, T_3 of the outer covering and T_4 of the soil. The calculation of thermal resistances from T_2 to T_4 requires specific information and computing processing, which is not usually available at the planning stages of a project. On the other hand, T_1 can be calculated with basic data found in open cable data sheets. Because of this, only T_1 is computed in this research to obtain an improved approximation of conductor temperature increase and associated losses. This approximation is good enough since the losses dependent on T_1 are at least an order of magnitude larger than the losses related to the T_2 to T_4 thermal resistances.

Since the power produced by the wind farm – and therefore the electrical loading of the cables – will be variable, the temperature of the cables may vary as a result, which in turn may affect the resistance of the cables. To improve the accuracy of the electrical loss calculations, some of the temperature effects have been included where possible. Eq. (3) describes the thermal resistance, T_1 in K m/W:

$$T_1 = \frac{pT}{2\,\pi}\; log\left(1 + 2\,\frac{t_1}{d_c}\right), \tag{3}$$

where pT is the thermal resistivity of the cable insulation (K m/W), t_1 is the thickness of the insulation (mm), and d_c is the diameter of the conductor (mm). Other similar factors are sometimes calculated for the inner sheath, outer sheath, and soil temperature but are considered to be negligible and thus are omitted from this study.

The resistance of a given cable at the maximum operating temperature of 90 °C, R_{90}, can be calculated as:

$$R_{90} = R_0(1 + \alpha_{20}(\theta_m - 20)), \tag{4}$$

where R_0 is the resistivity of the conductor, α_{20} is the temperature coefficient of resistance of the conductor material, and θ_m is the operating temperature of the cable conductor. The temperature increase of the cable conductor, α_θ, given the heat dissipation through the insulation, may be found through:

$$\alpha_\theta = T_1\;(0.5\;I^2\;R_{90}\;Loss_{DE}), \tag{5}$$

where $Loss_{DE}$ is the dielectric losses of the cable. The corresponding temperature dependent resistance, R_L, can be calculated as:

$$R_L = R_0\;(1 + \alpha_{20}(\alpha_\theta))\;. \tag{6}$$

Table 3
Key parameters of the cable set used in the inter-array cabling.

Position	Conductor area (mm^2)	Current rating (A)	Capacitance (μF/km)	Resistance (Ω/km)	Number of cables	Length of each cable (m)
1–3	240	530	0.20	0.0950	30	1640
4	300	599	0.21	0.0770	10	1640
5	500	780	0.25	0.0480	10	1640
6	630	886	0.28	0.0400	10	1640
7–8	1000	1173	0.33	0.0176	20	1640
9	1600	1465	0.40	0.0113	10	1640
10	1600	1465	0.40	0.0113	2	5420
11	1600	1465	0.40	0.0113	2	4340
12	1600	1465	0.40	0.0113	2	3306
13	1600	1465	0.40	0.0113	2	2378
14	1600	1465	0.40	0.0113	2	1738

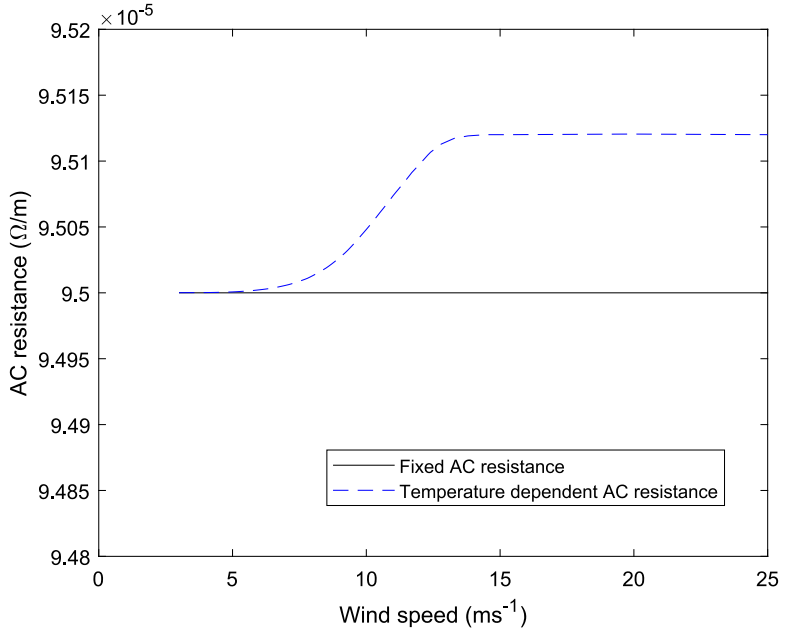

Fig. 22. Fixed-value resistance and temperature-dependent resistance R_L used in the calculations.

An example of the change in cable resistance can be seen in Fig. 22, comparing a single value AC resistance of a cable with a temperature-dependent AC resistance (due to different wind speeds leading to different electrical loading and, therefore different levels of cable heating). The resultant temperature-dependent R_L is then used to calculate the electrical losses.

3.4. Wind power economics

This section presents the methodology employed to calculate the CAPEX associated with reactive power compensation, array cables, and other costs, as well as the OPEX for the chosen offshore wind farm sites.

3.4.1. CAPEX associated with electrical works

3.4.1.1 Array cable For submarine cables, the following capital cost formula can be used (Lundberg, 2003; Dicorato et al., 2011):

$$C_c = \alpha + \beta\, e^{\gamma\, I_n/10^5} \quad [\text{k€/km}]\,, \tag{7}$$

where I_n represents cable ampacity (A), and α, β, and γ are coefficients depending on nominal voltage level.

Linear interpolation was used to approximate the parameters for a 66 kV cable based on the values determined in the study by Lundberg for 22–220 kV cables (Lundberg, 2003). The parameters for the 66 kV cable were calculated as $\alpha = 117.96$, $\beta = 59.17$ and $\gamma = 282.73$. Using these values and the array cable lengths and the number of parallel inter-array cables shown in Table 3, a total array cable CAPEX of € 384,909,034 for each of seven sites was calculated (since the array cable layouts and lengths were assumed identical across all sites). As the Eq. (7) was determined based on the value of money in 2011, a normalisation factor of 1.2706 was used to obtain the current value of money in 2023 based on cumulative inflation in EUR from 2011 to 2023.

3.4.1.2 Export cable A set of three XLPE, 2500 mm, segment stranded, copper-conductor, aluminium sheath 245 kV export cables (operating at 220 kV) were assumed for each site. The capacitance for this type of cable is 0.27 μF/km (LS Cable, 2008). Other technical characteristics of the cable, including the DC conductor resistance, can also be found in LS Cable (2008). The cost per single cable is 575 €/m. This cost was adapted from the indicative costs reported in ENTSO-e (2011) for mass-impregnated insulated subsea cables.

3.4.1.3 Reactive power compensation Reactive power compensation stations are used to reduce cable capacitance-related reactive power losses, which become prohibitively large for long-distance offshore cables. The CAPEX of the stations depends on their number and location. Based on the level of the power export, a detailed analysis can be performed to find the best trade-off between cost and loss reduction for compensation stations; one example of such analysis can be found in Dakic et al. (2021). Although the purpose of this paper is not to develop a detailed compensation station selection methodology, it is possible to detect trends in station selection based on academic studies and industrial practices.

Table 4
Technical specifications of reactive power calculations.

Site name	Cable length (km)	Capacitance per export cable C_T (μF)	Reactive power Q_T (MVAR)
Sørlige Nordsjø I	235	63.45	482.39
Sørlige Nordsjø II	234	63.18	480.34
Gimsøy Nord	18	4.86	36.95
Nordmela	20	5.40	41.05
Auvær	37	9.99	75.95
Vannøya Nordøst	23	6.21	47.21
Sandskallen-Sørøya Nord	54	14.58	110.85

Table 5
Reactive power compensation parameters used for the CAPEX calculations. P_c: coefficient for the proportional cost, F_c: coefficient for fixed cost.

Location	P_c (M€/MVAR)	F_c (M€/MVAR)
Onshore	0.0105	0.8312
Middle offshore	0.0158	12.4400
Offshore substation	0.1558	1.2400

The total reactive power compensation Q_T can be calculated to match the total capacitance C_T per three-phase export cable set using the formula:

$$Q_T = V^2 2\pi f C_T \quad [\text{VAR}]\,, \tag{8}$$

where V is the nominal transmission voltage in kV, and f is the transmission frequency in Hz. For each site, a three-phase 220 kV (phase-to-phase) export cable with a capacitance of 0.27 μF/km was chosen, as mentioned in Section 3.4.1.2. The cable length is assumed to equal the minimum distance to the nearest grid connection point for each site (see Section 4.1). The cable length, total capacitance, and the reactive power compensation for each site are presented in Table 4.

Indicative cost of reactive power compensation can be obtained from reports such as ENTSO-e (2011) and ESO (2013), and from academic papers such as Dakic et al. (2021) and Guiping et al. (2015) such that:

$$C_{react} = P_c \cdot Q_T + F_c \quad [\text{M€}]\,, \tag{9}$$

where C_{react} is the total cost of reactive power compensation, P_c is the coefficient for the proportional cost in M€/MVAR and F_c is the coefficient for fixed cost in M€/MVAR. The values of P_c and F_c are dependent on the location of the reactor. Their cost for onshore, middle offshore, and offshore substations are shown in Table 5.

In general terms, for offshore wind farms with a distance to the nearest connection point below 50 km, a single onshore compensation station can be used to comply with power factor requirements, as illustrated in Fig. 23(a). For distances between 50 km and 100 km, two compensation stations, one onshore and one offshore, as depicted in Fig. 23(b), can be used to keep a low level of reactive power-associated losses. For distances beyond 100 km, the use of three stations (one onshore, one offshore, and one at the middle point, as shown in Fig. 23(c)) is most likely needed to keep the losses within reasonable limits. This work adheres to these selection criteria to determine the number and location of stations in the analysed sites. Based on the configuration and location, the quantity of Q_T as outlined in Fig. 23 and the corresponding P_c and F_c are substituted into Eq. (9) to calculate the cost of each individual reactor.

3.4.2. CAPEX associated with turbine and foundation costs

As already mentioned in Section 3.3.2, the chosen turbine is the Vestas V164 9500, and the associated cost of 100 turbines was estimated to be 1.25 M€/MW (BloombergNEF, 2022), as also shown in Table 12. As provided in Section 3.2, bottom-fixed and floating foundation types are relevant for the chosen sites. Based on the average water depth of each site and installation costs provided in Fig. 2, a bottom-fixed foundation was chosen for sites with an average water depth less than 60 m, whereas a floating foundation was selected for depths at and above 60 m. The costs incorporate foundation types, platforms, moorings, anchors, and other relevant items. To keep the calculations simple, a hybrid foundation approach, as mentioned in the site descriptions (Section 3.2), was not adopted.

3.4.3. CAPEX associated with other costs

CAPEX considers a range of crucial costs for successful project execution. Project development is an essential aspect of this, encompassing all the expenses related to planning, designing, and ensuring the feasibility of the wind farm. A contingency scenario serves as a preparation strategy for potential unforeseen events or challenges that could arise during the implementation or operational phases. Insurance plays a vital role in offering financial protection against potential damages or losses, given the inherent risks associated with offshore operations. The installation costs account for setting up the wind turbines and other necessary infrastructure offshore. A significant part of the budget is also dedicated to the mooring system, a crucial aspect in offshore wind farms to ensure the stability and safety of the structures in the harsh marine environment. Collectively, these elements contribute to the total CAPEX, indicating the comprehensive investment needed for an offshore wind farm project. The costs mentioned are collectively represented under "other costs" in Table 12, and are presumed to be identical for each site. While a more detailed, site-specific analysis could provide further insight, such an approach exceeds the scope of this current study.

3.4.4. OPEX associated with foundation type and site conditions

The OPEX benchmark study presented in Wind (2023) reveals the market average as of 2020 as 135 k€/MW/yr, with a min–max range of 80–250 k€/MW/yr. The study anticipates a decrease in costs to the range of 41–82 k€/MW/yr, with an average of 61 k€/MW/yr, following a downward trend with an average year-on-year decrease of 2.5% based on the lifetime OPEX/MW profile for a 60-project sample. Another source reported a very similar finding, i.e., an OPEX of 131 k€/MW/yr and 115 k€/MW/yr for floating and fixed-bottom concepts, respectively (Bjerkseter and Ågotnes, 2013).

Annual OPEX/MW levels are highly dependent on the country of origin. According to the report by Wind (2023), analysing OPEX of European offshore wind farms revealed that OPEX/MW levels are correlated with the average distance to shore. However, it is important to note that other factors, such as the number of turbines, O&M strategy, logistical setup, etc., can also affect the OPEX/MW level. Based on the chosen foundation types, the site conditions (mild, moderate, and severe), the country of origin of the wind farm, and other conditions, six different empirical formulae were provided in Beiter et al. (2016).

Table 6 shows six empirical OPEX formulae as a function of the site condition and the foundation type. Site conditions consist of three categories, namely, mild, moderate, and severe, based on relevant spatial parameters, e.g., logistical distances and metocean conditions such as wind speed, water depth, distance to the coast, and wave height. We classified the severity of the site conditions as depicted in Table 7 based on the logistical distances and metocean conditions. The details on the water depth and other site-related information are provided in Section 4.1.

3.5. Proposed decision-making approach

In the following part, preliminaries of trigonometric norms and their extensions in the fuzzy domain are presented. After the presentation of the preliminary section, the fuzzy OPA-TRWA multicriteria framework, which was used for the evaluation of the wind farm sites, is shown.

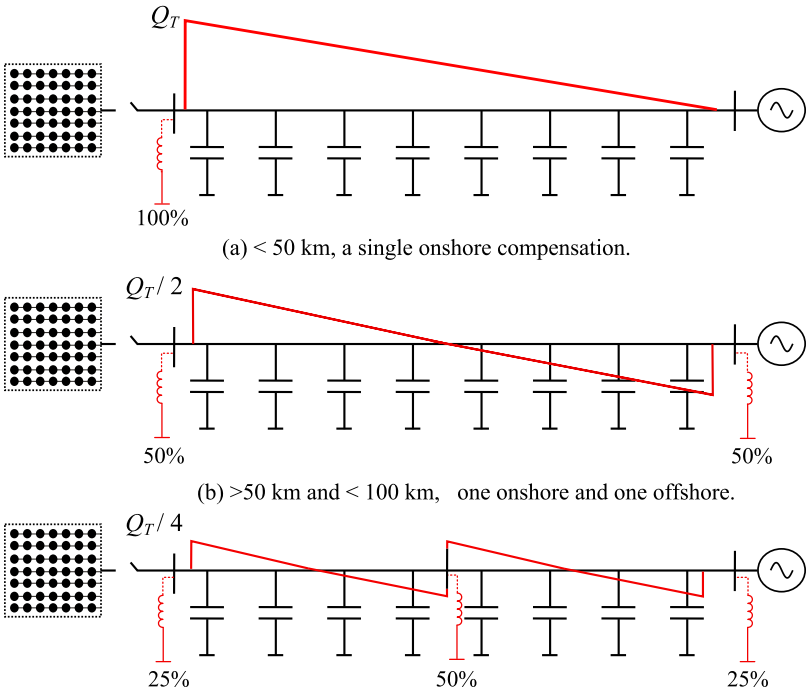

Fig. 23. Reactive power along a non-loaded HVAC cable for various reactor locations.
Source: Adapted from Dakic et al. (2021).

Table 6
OPEX formulae based on foundation type and site conditions (Beiter et al., 2016).

Foundation type	Site conditions		
	Mild	Moderate	Severe
Bottom-fixed (k€/yr)	$OPEX = 5.6691 \cdot ln(D) + 63.75$	$OPEX = 4.2876 \cdot ln(D) + 71.03$	$OPEX = 2.4501 \cdot ln(D) + 87.26$
Floating (k€/yr)	$OPEX = 5.8752 \cdot ln(D) + 53.72$	$OPEX = 4.4694 \cdot ln(D) + 65.77$	$OPEX = 4.0480 \cdot ln(D) + 117.64$

Table 7
Site conditions based on the logistical distances and metocean conditions.

Site	Foundation type	Site conditions
Sørlige Nordsjø I	Floating	Moderate
Sørlige Nordsjø II	Floating	Moderate
Gimsøy Nord	Bottom-fixed	Mild
Nordmela	Bottom-fixed	Moderate
Auvær	Bottom-fixed	Moderate
Vannøya Nordøst	Floating	Moderate
Sandskallen-Sørøya Nord	Floating	Moderate

3.5.1. Trigonometric t-norm and t-conorm

Definition 1. Suppose that ∂_1 and ∂_2 meet the condition that $(\partial_1, \partial_2) \in [0,1]$, then we can define the trigonometric T-norm and T-conorm between ∂_1 and ∂_2 as follows (Hu et al., 2015):

$$\Delta_D(\partial_1, \partial_2) = \frac{2}{\pi} arcsin\left(sin(\pi\partial_1/2) sin(\pi\partial_2/2)\right) \tag{10}$$

$$\Delta_D^c(\partial_1, \partial_2) = \frac{2}{\pi} arccos\left(cos(\pi\partial_1/2) cos(\pi\partial_2/2)\right) \tag{11}$$

where $(\partial_1, \partial_2) \in [0,1]$.

Then, based on the definition of trigonometric T-norm and T-conorm, we can define some trigonometric operational lows of fuzzy numbers $\tilde{\psi}_1 = (\psi_1^l, \psi_1^m, \psi_1^u)$ and $\tilde{\psi}_2 = (\psi_2^l, \psi_2^m, \psi_2^u)$.

Definition 2. Let us assume that $\tilde{\psi}_1 = (\psi_1^l, \psi_1^m, \psi_1^u)$ and $\tilde{\psi}_2 = (\psi_2^l, \psi_2^m, \psi_2^u)$ represent fuzzy numbers, where ψ_1^l and ψ_2^l represent lower limit, ψ_1^u and ψ_2^u represent upper limit, while ψ_1^m and ψ_2^m represent modal values of fuzzy numbers. Also, suppose that $\upsilon > 0$, $f(\tilde{\psi}_1) = \tilde{\psi}_1 / (\tilde{\psi}_1 + \tilde{\psi}_2)$ and $f(\tilde{\psi}_2) = \tilde{\psi}_2 / (\tilde{\psi}_1 + \tilde{\psi}_2)$; then, we can define the following operations:

(1) Addition "+"

$$\tilde{\psi}_1 + \tilde{\psi}_2 = \left(\left(\tilde{\psi}_1 + \tilde{\psi}_2\right) \frac{2}{\pi} arccos\left(cos(\pi f(\tilde{\psi}_1)/2) cos(\pi f(\tilde{\psi}_2)/2)\right)\right) \tag{12}$$

(2) Multiplication "×"

$$\tilde{\psi}_1 + \tilde{\psi}_2 = \left(\left(\tilde{\psi}_1 + \tilde{\psi}_2\right) \frac{2}{\pi} arcsin\left(sin(\pi f(\tilde{\psi}_1)/2) sin(\pi f(\tilde{\psi}_2)/2)\right)\right) \tag{13}$$

(3) Scalar multiplication $\upsilon \in (0, +\infty)$

$$\upsilon \times \tilde{\psi}_1 = \tilde{\psi}_1 \frac{2}{\pi} arccos\left(cos\left(\pi f(\tilde{\psi}_1)/2\right)^{\upsilon}\right) \tag{14}$$

(4) Power, where $\upsilon \in (0, +\infty)$

$$\tilde{\psi}_1^{\upsilon} = \tilde{\psi}_1 \frac{2}{\pi} arcsin\left(sin\left(\pi f(\tilde{\psi}_1)/2\right)^{\upsilon}\right) \tag{15}$$

3.5.2. Fuzzy OPA-TRWA multicriteria framework

The proposed decision-making procedure engaged researchers seasoned with over a decade of expertise in wind energy within both academic and industrial contexts. These experts assessed the impact of the criteria, identified in Section 3.1, for each site, drawing upon their engineering judgement and extensive observations of the societal and energy political landscape.

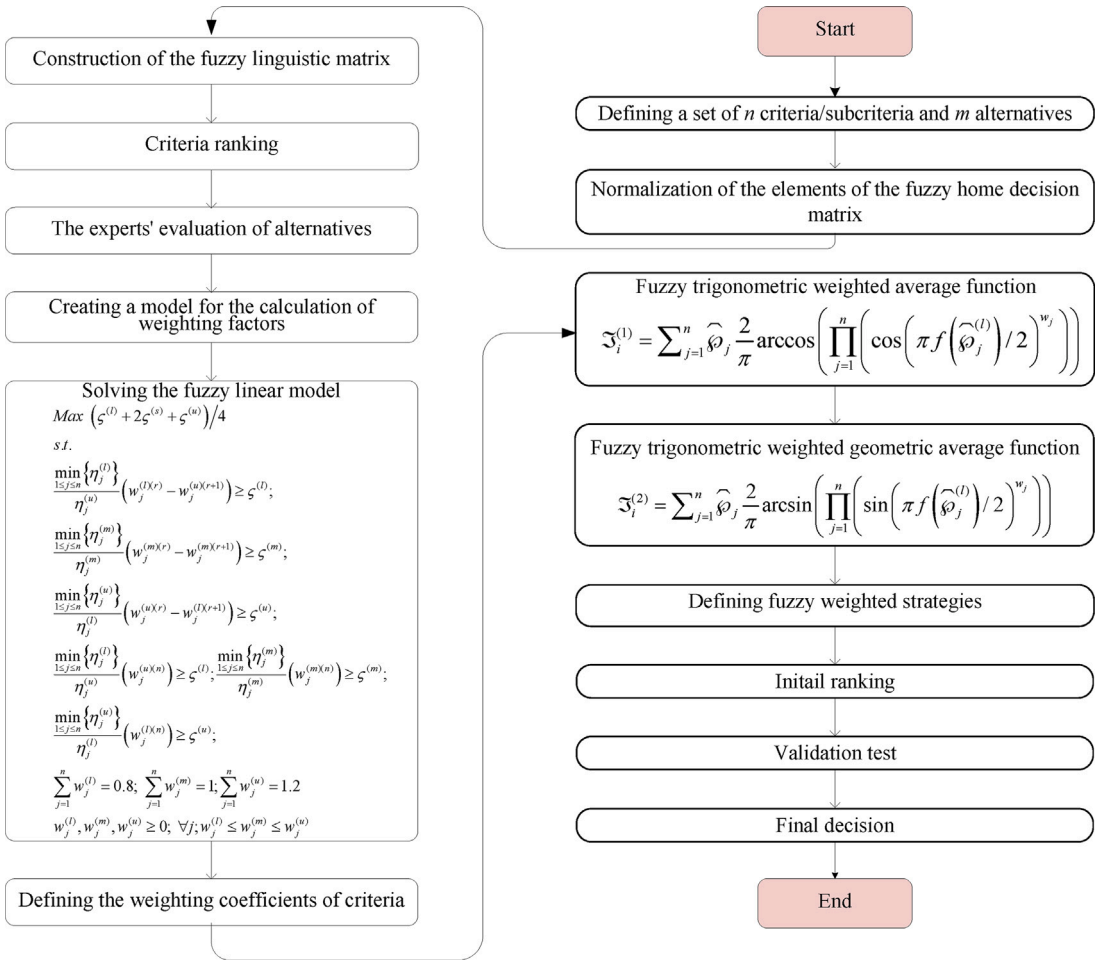

Fig. 24. Process diagram of the proposed fuzzy OPA-TRWA multicriteria framework.

The multicriteria framework presented in this study is realised through two phases, as indicated in Fig. 24. In the first phase, the fuzzy linear OPA model is implemented, which is used to define the weighting coefficients of the criteria, where experts' evaluations of alternatives are used. The fuzzy OPA model's fuzzy weight coefficients represent the second stage's input parameters. In the second phase, based on the fuzzy weight of the criteria, the set of alternatives is evaluated using the fuzzy TRWA algorithm.

Fuzzy OPA methodology was used to determine the weighting coefficients of the criteria since the OPA method is based on defining the weighting coefficients based on objective expert preferences. This eliminates the problem of a limited range of predefined scales for comparing criteria used in other subjective models. Furthermore, the functions of sine trigonometry have been implemented within the TRWA model for evaluation, which enables the correct presentation of information around the origin and contributes to the objective representation of the decision-makers' preferences.

To present the mathematical foundations of the fuzzy OPA-TRWA methodology, the following part presents basic assumptions and notations. First, suppose that a set of m alternatives A_i $(i = 1, 2, \ldots, m)$ is defined, which needs to be ranked based on a predefined set of n criteria C_j $(j = 1, 2, \ldots, n)$. Also, let us assume that fuzzy scales are defined for the evaluation of criteria/alternatives that were used for evaluation by e experts. Then, based on the preliminary settings, we can define the mathematical foundations of the fuzzy OPA-TRWA methodology.

3.5.2.1. Fuzzy OPA algorithm The methodological framework of the fuzzy OPA model involves defining the rank of criteria based on expert evaluations and generating a fuzzy linear model for calculating the weighting coefficients of the criteria.

Step 1: Generation of the fuzzy matrix of expert assessments. Expert assessments on the significance of criteria are presented in the assessment matrix $\aleph^t = \left[\tilde{\eta}^t_{C_j}\right]_{nx1}$, $\tilde{\eta}^t_{C_j} = \left(\tilde{\eta}^{(l)t}_{C_j}, \tilde{\eta}^{(m)t}_{C_j}, \tilde{\eta}^{(u)t}_{C_j}\right)$, $(1 \le t \le e)$. To define the final ranking of the criteria, it is necessary to perform a fusion of expert assessments that are shown in the aggregated matrix $\aleph^t = \left[\tilde{\eta}^t_{C_j}\right]_{nx1}$. Thus, we get the final rank of the criterion $w_l^{(1)} \ge w_l^{(2)} \ge \cdots \ge w_l^{(r)} \ge w_l^{(r+1)} \ge \cdots \ge w_l^{(n)}$, where $w_l^{(r)}$ represents the lth criterion assigned the rank r. Since it is necessary that the ranked weight coefficients satisfy the condition that $\tilde{w}_l^{(1)} - \tilde{w}_l^{(2)} \ge 0; \tilde{w}_l^{(2)} - \tilde{w}_l^{(3)} \ge 0; \ldots; \tilde{w}_l^{(r)} - \tilde{w}_l^{(r+1)} \ge 0; \ldots; \tilde{w}_l^{(n-1)} - \tilde{w}_l^{(n)} \ge 0$. Then, we can define the following condition:

$$\tilde{\eta}^r_l\left(\tilde{w}_l^{(r)} - \tilde{w}_l^{(r+1)}\right) \ge 0; \quad \forall_l \tag{16}$$

Step 2: Fuzzy OPA linear model. Based on the assessment matrix $\aleph^t = \left[\tilde{\eta}^t_{C_j}\right]_{nx1}$ and Eq. (16), a fuzzy linear model for determining the

weighting coefficients of the criteria, Eq. (17), was defined.

$$\begin{cases} Max\left(\varsigma^{(l)} + 2\varsigma^{(m)} + \varsigma^{(u)}/4\right) \\ s.t. \\ \frac{min_{1\le j\le n}\left\{\eta_j^{(l)}\right\}}{\eta_j^{(u)}}\left(w_j^{(l)(r)} - w_j^{(u)(r+1)}\right) \ge \varsigma^{(l)}; \\ \frac{min_{1\le j\le n}\left\{\eta_{\mathbb{C}_j}^{(m)}\right\}}{\eta_{\mathbb{C}_j}^{(m)}}\left(w_j^{(m)(r)} - w_j^{(m)(r+1)}\right) \ge \varsigma^{(m)}; \\ \frac{min_{1\le j\le n}\left\{\eta_{\mathbb{C}_j}^{(u)}\right\}}{\eta_{\mathbb{C}_j}^{(l)}}\left(w_j^{(u)(r)} - w_j^{(l)(r+1)}\right) \ge \varsigma^{(u)}; \frac{min_{1\le j\le n}\left\{\eta_{\mathbb{C}_j}^{(l)}\right\}}{\eta_{\mathbb{C}_j}^{(u)}}\left(w_j^{(u)(n)}\right) \ge \varsigma^{(l)}; \\ \frac{min_{1\le j\le n}\left\{\eta_{\mathbb{C}_j}^{(m)}\right\}}{\eta_{\mathbb{C}_j}^{(m)}}\left(w_j^{(m)(n)}\right) \ge \varsigma^{(m)}; \frac{min_{1\le j\le n}\left\{\eta_{\mathbb{C}_j}^{(u)}\right\}}{\eta_{\mathbb{C}_j}^{(l)}}\left(w_j^{(l)(n)}\right) \ge \varsigma^{(u)}; \\ \sum_{j=1}^{n} w_j^{(l)} = 0.8; \sum_{j=1}^{n} w_j^{(m)} = 1; \sum_{j=1}^{n} w_j^{(u)} = 1.2; \quad \forall_j \\ w_j^{(l)}, w_j^{(m)}, w_j^{(u)} \ge 0; \quad \forall_j \\ w_j^{(l)} \le w_j^{(m)} \le w_j^{(u)} \end{cases} \tag{17}$$

where $\tilde{w}_j = \left(w_j^{(l)}, w_j^{(m)}, w_j^{(u)}\right)$ represents fuzzy weight coefficients.

3.5.2.2. Fuzzy TRWA model Fuzzy TRWA methodology is implemented through three steps, which are presented in the next part:

Step 1: Constructing the initial decision matrix. The values of alternatives A_i $(i = 1, 2, \ldots, m)$ within the evaluation criteria C_j $(j = 1, 2, \ldots, n)$ are presented in the initial decision matrix $\mathbb{Q} = \left[\tilde{\partial}_{ij}\right]_{mxn}$. The elements of the initial decision matrix $\tilde{\partial}_{ij} = \left(\tilde{\partial}_{ij}^{l}, \tilde{\partial}_{ij}^{m}, \tilde{\partial}_{ij}^{u}\right)$ represent quantitative or qualitative information depending on the nature of the criteria. A fuzzy scale was used to present qualitative information, while quantitative values were obtained by measuring the performance of alternatives.

Since different measurement units represent the information in the initial decision matrix $\mathbb{Q} = \left[\tilde{\partial}_{ij}\right]_{mxn}$, it is necessary to perform their standardisation, which involves transforming the values of the initial decision matrix into the interval $[0, 1]$. Standardisation was performed using Eq. (18).

$$\hat{\partial}_{ij} = \begin{cases} \hat{\partial}_{ij} = \frac{\tilde{\partial}_{ij}}{\tilde{\partial}_j^+} & if \quad \in B, \\ \hat{\partial}_{ij} = -\frac{\tilde{\partial}_{ij}}{\tilde{\partial}_j^+} + max_{1\le i\le m}\left\{\frac{\tilde{\partial}_{ij}}{\tilde{\partial}_j^+}\right\} + min_{1\le i\le m}\left\{\frac{\tilde{\partial}_{ij}}{\tilde{\partial}_j^+}\right\} & if \quad \in C \end{cases} \tag{18}$$

where $\hat{\partial}_j^+ = max_{1\le i\le m}\left(\hat{\partial}_{ij}\right)$.

Step 2: Calculation of trigonometric fuzzy weighted alternative strategies. Fuzzy weighted sequences can be used to define a preliminary ranking of alternatives within a considered strategy. Trigonometric fuzzy weighted strategies are defined by applying non-linear functions of sine trigonometry, shown in Eqs. (19) and (20).

Theorem 1. *Let $\hat{\partial}_{ij}(j = 1, 2, \ldots, n; i = 1, 2, \ldots, m)$ represent the standardised elements of the initial decision matrix, and let $\tilde{w}_j = \left(\tilde{w}_1, \tilde{w}_2, \ldots, \tilde{w}_n\right)^T$ represent the fuzzy vector of weight coefficients of criteria. Then we can define the fuzzy trigonometric weighted average function $\mathfrak{F}_i^{(1)}$ as follows:*

$$\mathfrak{F}_i^{(1)} = \begin{bmatrix} \sum_{j=1}^{n} \hat{\wp}_j^{(l)} \frac{2}{\pi} arccos\left(\prod_{j=1}^{n}\left(cos\left(\pi f\left(\hat{\wp}_j^{(l)}\right)/2\right)^{w_j^{(l)}}\right)\right), \\ \sum_{j=1}^{n} \hat{\wp}_j^{(m)} \frac{2}{\pi} arccos\left(\prod_{j=1}^{n}\left(cos\left(\pi f\left(\hat{\wp}_j^{(m)}\right)/2\right)^{w_j^{(m)}}\right)\right), \\ \sum_{j=1}^{n} \hat{\wp}_j^{(u)} \frac{2}{\pi} arccos\left(\prod_{j=1}^{n}\left(cos\left(\pi f\left(\hat{\wp}_j^{(u)}\right)/2\right)^{w_j^{(u)}}\right)\right), \end{bmatrix} \tag{19}$$

where $f\left(\hat{\wp}_{ij}\right)$ represents the fuzzy additive fuzzy function of the standardised elements of the initial decision matrix. Then, $\mathfrak{F}_i^{(1)}$ represents the fuzzy trigonometric weighted average function.

Theorem 2. *Let $\hat{\partial}_{ij}(j = 1, 2, \ldots, n; i = 1, 2, \ldots, m)$ represent the standardised elements of the initial decision matrix, and let $\tilde{w}_j = \left(\tilde{w}_1, \tilde{w}_2, \ldots, \tilde{w}_n\right)^T$ represent the fuzzy vector of weight coefficients of criteria. Then, we can define the fuzzy trigonometric weighted geometric average function $\mathfrak{F}_i^{(2)}$ as follows:*

$$\mathfrak{F}_i^{(2)} = \begin{bmatrix} \sum_{j=1}^{n} \hat{\wp}_j^{(l)} \frac{2}{\pi} arcsin\left(\prod_{j=1}^{n}\left(sin\left(\pi f\left(\hat{\wp}_j^{(l)}\right)/2\right)^{w_j^{(l)}}\right)\right), \\ \sum_{j=1}^{n} \hat{\wp}_j^{(m)} \frac{2}{\pi} arcsin\left(\prod_{j=1}^{n}\left(sin\left(\pi f\left(\hat{\wp}_j^{(m)}\right)/2\right)^{w_j^{(m)}}\right)\right), \\ \sum_{j=1}^{n} \hat{\wp}_j^{(u)} \frac{2}{\pi} arcsin\left(\prod_{j=1}^{n}\left(sin\left(\pi f\left(\hat{\wp}_j^{(u)}\right)/2\right)^{w_j^{(u)}}\right)\right), \end{bmatrix} \tag{20}$$

where $f\left(\hat{\wp}_{ij}\right)$ represents the fuzzy additive fuzzy function of the standardised elements of the initial decision matrix. Then $\mathfrak{F}_i^{(2)}$ represents the fuzzy trigonometric weighted geometric average function:

$$\nabla_i = \left(\mathfrak{F}_i^{(1)} + \mathfrak{F}_i^{(2)}\right) \cdot e^{-\left(\zeta\left(-ln\left(f\left(\mathfrak{F}_i^{(1)}\right)\right)\right)^{\delta} + (1-\zeta)\left(-ln\left(f\left(\mathfrak{F}_i^{(2)}\right)\right)\right)^{\delta}\right)^{1/\delta}} \tag{21}$$

where ∇_i denotes final assessment score of the alternatives, $\delta \ge 1$, $\zeta \in [0, 1]$, $f\left(\mathfrak{F}_i^{(1)}\right) = \frac{\mathfrak{F}_i^{(1)}}{\mathfrak{F}_i^{(1)} + \mathfrak{F}_i^{(2)}}$ and $f\left(\mathfrak{F}_i^{(2)}\right) = \frac{\mathfrak{F}_i^{(2)}}{\mathfrak{F}_i^{(1)} + \mathfrak{F}_i^{(2)}}$.

The coefficient ζ is used to define the impact of strategies $\mathfrak{F}_i^{(1)}$ and $\mathfrak{F}_i^{(2)}$ in the aggregation function, Eq. (21). For values $0 \le \zeta < 0.5$, the influence of $\mathfrak{F}_i^{(2)}$ is favoured, while for $0.5 \le \zeta < 1$, the influence of $\mathfrak{F}_i^{(1)}$ is favoured. When defining the initial solution, it is recommended to adopt the value $\zeta = 0.5$, since this ensures the same intensity of influence of both functions ($\mathfrak{F}_i^{(1)}$ and $\mathfrak{F}_i^{(2)}$).

4. Results

The Results section is organised into two main parts. Firstly, the calculated and retrieved DM parameters are presented, and secondly, the outcomes of the DM framework are displayed.

4.1. Decision-making parameters

The following tables provide a summary of the performance of each of the seven sites against the 17 criteria outlined in Section 3.1.

4.1.1. Performance Criteria I: Wind power output

Table 8 shows the calculated mean wind speed, net AEY, and net CF of each of the seven sites based on the methods described in Section 3.1. Sørlige Nordsjø I and Sørlige Nordsjø II have the highest mean wind speeds, 10.60 m/s and 10.58 m/s, respectively, while Vannøya Nordøst has the lowest at 7.93 m/s. Correspondingly, Sørlige Nordsjø I and Sørlige Nordsjø II have the highest AEY; however, the lowest AEY is found at the Auvær site. With identical wind farm installed capacities across all seven sites, the net CF mirrors the net AEY. Sørlige Nordsjø II has the highest CF, followed by Sørlige Nordsjø I, Sandskallen-Sørøya Nord, Vannøya Nordøst, Gimsøy Nord, Nordmela, and Auvær, respectively.

4.1.2. Performance Criteria II: Site specific features

Table 9 summarises the performance of the sites considering the average water depth, distance to the nearest grid connection, distance to the coast, average wave height, and 50-year highest wave height. These data are retrieved from the NVE reports Berg et al. (2012) and NVE (2017) and supplementary report published by Multiconsult (2012). The average water depths range between 34 m at the Gimsøy Nord site to 89 m at the Sandskallen-Sørøya Nord site. While four of the sites have minimum water depths of approximately 0 m, the maximum depth of 221 m is seen at Sandskallen-Sørøya Nord. Most of the sites are relatively close to shore, between 0 km and 14 km; however, Sørlige Nordsjø I and Sørlige Nordsjø II are much further from shore at 149 km

Table 8
Performance Criteria I: (C1) mean wind speed, (C2) net annual energy yield, and (C3) net capacity factor of the seven sites.

Site	C1 Mean wind speed (m/s)	C2 Net AEY (GWh)	C3 Net capacity factor (%)
A_1–Sørlige Nordsjø I	10.60	3999.39	48.06
A_2–Sørlige Nordsjø II	10.58	4143.38	49.79
A_3–Gimsøy Nord	8.45	3095.31	37.19
A_4–Nordmela	8.19	3082.32	37.04
A_5–Auvær	8.13	2895.97	34.80
A_6–Vannøya Nordøst	7.93	3175.45	38.16
A_7–Sandskallen-Sørøya Nord	8.82	3441.67	41.36

Table 9
Performance Criteria II: (C4) average water depth (and min–max), (C5) distance to nearest grid connection, (C6) minimum distance to the coast, and (C7) average wave height (and 50-year highest wave) of the seven sites retrieved from Berg et al. (2012), Multiconsult (2012) and NVE (2017).

Site	C4 Avg. water depth (min, max) (m)	C5 Distance to the nearest grid connection (km)	C6 Min. distance to the coast (km)	C7 Average wave height (50-year highest wave) (m)
A_1–Sørlige Nordsjø I	65 (50–82)	235	149	2.1 (12.5)
A_2–Sørlige Nordsjø II	60 (53–70)	234	140	2.0 (12.9)
A_3–Gimsøy Nord	34 (0–118)	18	1	0.6 (12.8)
A_4–Nordmela	55 (0–152)	20	2	1.8 (12.8)
A_5–Auvær	45 (0–150)	37	11	2.0 (14.6)
A_6–Vannøya Nordøst	63 (0–214)	23	0	0.8 (12.0)
A_7–Sandskallen-Sørøya Nord	89 (23–221)	54	14	2.1 (14.1)

Table 10
Costs of reactive power compensation based on the distance from the nearest grid connection point.

Site	Cost of reactive power onshore (M€)	Cost of reactive power middle offshore (M€)	Cost of reactive power offshore (M€)	Total cost of reactive power (M€)
A_1–Sørlige Nordsjø I	2.10	16.24	3.14	**21.48**
A_2–Sørlige Nordsjø II	2.09	16.23	3.14	**21.45**
A_3–Gimsøy Nord	1.22	0	0	**1.22**
A_4–Nordmela	1.26	0	0	**1.26**
A_5–Auvær	1.63	0	0	**1.63**
A_6–Vannøya Nordøst	1.33	0	0	**1.33**
A_7–Sandskallen-Sørøya Nord	1.41	0	2.12	**3.53**

and 140 km, respectively. A similar pattern is seen in the distances to the nearest grid connection. Five of the seven sites have average wave heights of 1.8–2.1 m, but Gimsøy Nord and Vannøya Nordøst have much lower average wave heights of 0.6 m and 0.8 m, respectively. Extreme wave heights (50-year highest wave) for all sites are at least 12 m, with Auvær and Sandskallen-Sørøya Nord exhibiting extreme wave heights of 14.6 m and 14.1 m, respectively.

4.1.3. Performance Criteria III: Cost of electrical works and losses

The costs for the electrical works encompass reactive power compensation, inter-array cabling, and the export cable. Table 10 displays the total cost of reactive power compensation for the analysed sites. The corresponding cost of each station was determined using Eq. (9), based on the amount of Q_T to be compensated. As indicated in the table, for Sørlige Nordsjø I and II, where the distance to the nearest grid connection point exceeds 200 km, three stations – one onshore ($Q_T/4$), one offshore ($Q_T/4$), and one at the midpoint ($Q_T/2$), as illustrated in Fig. 23(c) – were considered, rendering them the most costly sites for reactive power compensation. Sandskallen-Sørøya Nord, being the third furthest site from the nearest grid connection at 54 km, necessitates two compensation stations: one onshore and one offshore, each compensating ($Q_T/2$), as depicted in Fig. 23(b). For the remaining sites, which are all situated under 50 km from the grid connection, a single onshore compensation station was considered, as shown in Fig. 23(a).

Given that the number of turbines and their array configurations are identical for each site, as depicted in Fig. 21, the inter-array cabling cost is uniform across all sites, detailed in Table 11. Additionally, the resulting export cable costs, calculated relative to the proximity to the nearest grid connection point for each site (refer to Section 4.1), are also outlined in Table 11. The total cost for reactive power, presented in Table 10, is incorporated into Table 11 to display the aggregate cost of electrical works.

Table 12 compiles all the cost components that contribute to the overall CAPEX, explicitly detailing the expenditure for 100 Vestas V164 9500 turbines, the total electrical work costs presented in Table 11 in million EUR per megawatt (M€/MW), and other costs as outlined in Section 3.4.3.

Table 13 presents the aggregate CAPEX, OPEX, wake losses and electrical losses of the seven sites. The CAPEX of all sites ranges between 3.14 M€/MW at the Gimsøy Nord site to 3.65 M€/MW at the Sørlige Nordsjø I site, a relative increase of 16.6%. The OPEX follows a similar relationship, with Gimsøy Nord having the lowest cost of 80.13 k€/MW/yr and Sørlige Nordsjø I having the highest cost of 90.17 k€/MW/yr. It is noteworthy that the most comprehensive study, conducted by Multiconsult for NVE (Multiconsult, 2012), which analysed the same sites among others, also reported CAPEX costs in the range of 26–31 MNOK/MW (approximately 2.6–3.1 MEUR/MW). This range aligns closely with the one calculated in our work.

Wake losses across the seven sites vary greatly, from 7.97% at the Sørlige Nordsjø II site to more than double that at 16.02% at the Nordmela site, highlighting the impact of the wind rose distributions presented earlier. With the exceptions of Nordmela (16.02%) and Auvær (15.84%), all other sites exhibit wake losses of less than 11%. Owing to the reactive power compensation, electrical losses for the seven sites are maintained at relatively low levels. Losses are notably minimal for the five sites closest to the shore, ranging from 0.41–0.65%. However, the electrical losses for Sørlige Nordsjø I and Sørlige

Table 11
CAPEX associated with electrical works.

Site	Inter-array cabling (M€)	Export cable (M€)	Reactive power compensation (M€)	Total cost of electrical works (M€)
A_1–Sørlige Nordsjø I	384.91	405.38	21.48	**811.77**
A_2–Sørlige Nordsjø II	384.91	403.65	21.45	**810.01**
A_3–Gimsøy Nord	384.91	31.05	1.22	**417.18**
A_4–Nordmela	384.91	34.50	1.26	**420.67**
A_5–Auvær	384.91	63.83	1.63	**450.36**
A_6–Vannøya Nordøst	384.91	39.67	1.33	**425.91**
A_7–Sandskallen-Sørøya Nord	384.91	93.15	3.53	**481.59**

Table 12
CAPEX associated with turbine, foundation and other costs.

Site	Turbine cost (M€/MW)	Total cost of electrical works (M€/MW)	Foundation costs (M€/MW)	Other costs (M€/MW)
A_1–Sørlige Nordsjø I	1.25	0.85	0.52	1.03
A_2–Sørlige Nordsjø II	1.25	0.85	0.52	1.03
A_3–Gimsøy Nord	1.25	0.44	0.42	1.03
A_4–Nordmela	1.25	0.44	0.44	1.03
A_5–Auvær	1.25	0.47	0.46	1.03
A_6–Vannøya Nordøst	1.25	0.45	0.52	1.03
A_7–Sandskallen-Sørøya Nord	1.25	0.51	0.52	1.03

Table 13
Performance Criteria III: (C8) capital expenditure, (C9) operational expenditure, (C10) wake losses, and (C11) electrical losses of the seven sites.

Site	C8 CAPEX (M€/MW)	C9 OPEX (k€/MW/yr)	C10 Wake losses (%)	C11 Electrical losses (%)
A_1–Sørlige Nordsjø I	3.65	90.17	8.43	2.12
A_2–Sørlige Nordsjø II	3.65	90.15	7.97	2.10
A_3–Gimsøy Nord	3.14	80.13	10.95	0.41
A_4–Nordmela	3.16	83.87	16.02	0.42
A_5–Auvær	3.21	86.51	15.84	0.54
A_6–Vannøya Nordøst	3.25	80.79	10.22	0.46
A_7–Sandskallen-Sørøya Nord	3.31	83.60	9.67	0.65

Table 14
Performance Criteria IV: (C12) technical-financial suitability, (C13) impact on fish, (C14) impact on fisheries, (C15) impact on marine species, (C16) impact on sea birds, and (C17) legislative focus of the seven sites (where 0: none, 1: very low, …, 5: very high).
Source: Retrieved from Berg et al. (2012).

Site	C12 Technical-financial suitability	C13 Impact on fish	C14 Impact on fisheries	C15 Impact on marine species	C16 Impact on sea birds	C17 Legislative focus
A_1–Sørlige Nordsjø I	4	1	1	1	2	5
A_2–Sørlige Nordsjø II	4	3	1	0	2	5
A_3–Gimsøy Nord	5	1	3	3	4	1
A_4–Nordmela	5	1	4	3	3	1
A_5–Auvær	3	1	3	3	3	3
A_6–Vannøya Nordøst	3	1	3	3	3	3
A_7–Sandskallen-Sørøya Nord	3	1	4	1	2	5

Nordsjø II are significantly higher, at 2.12% and 2.10%, respectively, primarily due to their considerably greater distances to shore and grid connections.

Individual expert assessments are compiled in the assessment matrix to determine the final criteria ranking. The aggregated assessment matrix and ranking of criteria are depicted in Table 16.

4.1.4. Performance Criteria IV: Score-based assessments of the sites

Table 14 contains the remaining six performance criteria that utilise a score-based system to assess the suitability of the sites. Technical-financial suitability, impact on fish, impact on fisheries, impact on marine species, impact on sea birds, and governmental priority are all considered. Each site is scored on a scale of 0 to 5 against each criterion, with a score of 1 representing "Very Low" and 5 representing "Very High". It is worth noting that for the four criteria starting "Impact on..." (C13, C14, C15, and C16), a 'good' score is a lower number, while for the two remaining criteria (C12 and C17), a 'good' score is a higher number. Governmental priority is the category showing the largest spread of scores, ranging from 1 to 5; all other categories show a closer set of scores across sites.

It should be noted that these scores were directly extracted from the NVE's report (Appendix E) Berg et al. (2012). Consequently, expert opinions for C12–C17 were not solicited. Instead, we adapted them by converting NVE's scale (from 0 to 5) to our linguistic terms, which utilise 9 scales, as illustrated in Table 15.

Based on the comprehensive work performed by Berg et al. (2012), the sites Gimsøy Nord and Nordmela attained the highest scores (5) in technical-financial suitability, indicating optimal conditions or prospects for wind power development from a technical-financial perspective. Conversely, Auvær, Vannøya Nordøst, and Sandskallen-Sørøya Nord present moderate suitability, each scoring a 3.

Table 15
Fuzzy linguistic variables.

NVE's scale (Berg et al., 2012)	Linguistic terms	Linguistic values of TrFNs
0	Absolutely low (AL)	(1, 1.5, 2.5)
1	Very low (VL)	(1.5, 2.5, 3.5)
	Low (L)	(2.5, 3.5, 4.5)
2	Medium low (ML)	(3.5, 4.5, 5.5)
	Equal (E)	(4.5, 5.5, 6.5)
3	Medium high (MH)	(5.5, 6.5, 7.5)
	High (H)	(6.5, 7.5, 8.5)
4	Very high (VH)	(7.5, 8.5, 9.5)
5	Absolutely high (AH)	(8.5, 9, 10)

Table 16
The weights of criteria based on the expert assessments.

Criteria	$\tilde{\eta}_{C_j}$	Rank
C1	(7.67,8.58,9.58)	6
C2	(8.5,9,10)	1
C3	(7.83,8.58,9.58)	5
C4	(6.17,7.17,8.17)	12
C5	(7,8,9)	8
C6	(4.83,5.83,6.83)	16
C7	(4.17,5.17,6.17)	17
C8	(8.33,8.92,9.92)	2
C9	(8.17,8.83,9.83)	3
C10	(7.17,8.17,9.17)	7
C11	(7,8,9)	8
C12	(8.17,8.83,9.83)	3
C13	(6,7,8)	13
C14	(5.67,6.67,7.67)	15
C15	(6.33,7.33,8.33)	11
C16	(6,7,8)	13
C17	(6.83,7.83,8.83)	10

$\tilde{\eta}_{C_j} = \left(\tilde{\eta}_{C_j}^{(l)}, \tilde{\eta}_{C_j}^{(m)}, \tilde{\eta}_{C_j}^{(u)}\right)$, $(j = 1, 2, \ldots, 17)$ represent the elements of the aggregated assessment matrix.

Sørlige Nordsjø II showed the highest impact on fish with a score of 3, while all other sites generally exhibit low or very low impact, signifying minimal disturbance to fish habitats and populations. Notably, Nordmela and Sandskallen-Sørøya Nord scored 4 in terms of their impact on fisheries, suggesting a considerable influence on fishing activities or zones. Gimsøy Nord and Auvær also indicate notable impacts, scoring 3.

Most sites depict a moderate impact on marine species, scoring 3. An exception is Sørlige Nordsjø II, which appears to have no or negligible impact, obtaining a score of 0.

Gimsøy Nord manifested the highest impact on sea birds with a score of 4, potentially indicating a significant interference with bird habitats or migration patterns. Most other sites portrayed low to moderate impacts.

Based on the criteria and additional quantitative data explored in Drivenes et al. (2010), Berg et al. (2012) and Multiconsult (2012), there is a notably high governmental or legislative focus (score of 5) on Sørlige Nordsjø I, Sørlige Nordsjø II, and Sandskallen-Sørøya Nord, spotlighting these sites as potential areas of interest or priority for governmental bodies or policies.

4.2. Results of DM framework

Using the proposed fuzzy OPA-TRWA methodology, the investment decision for seven Norwegian offshore wind power projects was prioritised based on a variety of multidisciplinary factors. This strategy used expert input, as illustrated in Fig. 4. Seventeen criteria were identified, which were grouped into four clusters, as shown in Fig. 5. In the following part, the definition of the weighting coefficients of the criteria is presented using the fuzzy OPA algorithm.

4.2.1. Fuzzy OPA algorithm

The fuzzy OPA algorithm is based on the application of a fuzzy linear model. Defining the constraints and generating the fuzzy linear model is shown in the next part:

Step 1: The fuzzy matrix of expert evaluations includes six experts who participated in the research. The experts used a fuzzy scale to present the assessments, Table 15.

Step 2: Based on the elements of the aggregated assessment matrix and Eq. (16), a fuzzy linear model, Eq. (17), was defined, which was used to define the weighting coefficients $\tilde{w}_j = \left(\tilde{w}_j^{(l)}, \tilde{w}_j^{(m)}, \tilde{w}_j^{(u)}\right)$.

$$Max\ \left(\varsigma^{(l)} + 2\varsigma^{(m)} + \varsigma^{(u)}/4\right)$$

s.t.

$$\begin{cases}
0.4167 \cdot \left(w_2^{(l)} - w_8^{(u)}\right) \geq \zeta^{(l)}; 0.4630 \cdot \left(w_2^{(m)} - w_8^{(m)}\right) \geq \zeta^{(m)}; \\
0.4902 \cdot \left(w_2^{(u)} - w_8^{(l)}\right) \geq \zeta^{(u)}; \\
0.4202 \cdot \left(w_8^{(l)} - w_9^{(u)}\right) \geq \zeta^{(l)}; 0.4673 \cdot \left(w_8^{(m)} - w_9^{(m)}\right) \geq \zeta^{(m)}; \\
0.5000 \cdot \left(w_8^{(u)} - w_9^{(l)}\right) \geq \zeta^{(u)}; \\
0.4237 \cdot \left(w_9^{(l)} - w_{12}^{(u)}\right) \geq \zeta^{(l)}; 0.4717 \cdot \left(w_9^{(m)} - w_{12}^{(m)}\right) \geq \zeta^{(m)}; \\
0.5102 \cdot \left(w_9^{(u)} - w_{12}^{(l)}\right) \geq \zeta^{(u)}; \\
0.4237 \cdot \left(w_{12}^{(l)} - w_3^{(u)}\right) \geq \zeta^{(l)}; 0.4717 \cdot \left(w_{12}^{(m)} - w_3^{(m)}\right) \geq \zeta^{(m)}; \\
0.5102 \cdot \left(w_{12}^{(u)} - w_3^{(l)}\right) \geq \zeta^{(u)}; \\
0.4348 \cdot \left(w_3^{(l)} - w_1^{(u)}\right) \geq \zeta^{(l)}; 0.4854 \cdot \left(w_3^{(m)} - w_1^{(m)}\right) \geq \zeta^{(m)}; \\
0.5319 \cdot \left(w_3^{(u)} - w_1^{(l)}\right) \geq \zeta^{(u)}; \\
0.4348 \cdot \left(w_1^{(l)} - w_{10}^{(u)}\right) \geq \zeta^{(l)}; 0.4854 \cdot \left(w_1^{(m)} - w_{10}^{(m)}\right) \geq \zeta^{(m)}; \\
0.5319 \cdot \left(w_1^{(u)} - w_{10}^{(l)}\right) \geq \zeta^{(u)}; \\
\ldots \\
0.6098 \cdot \left(w_6^{(l)} - w_7^{(u)}\right) \geq \zeta^{(l)}; 0.7143 \cdot \left(w_6^{(m)} - w_7^{(m)}\right) \geq \zeta^{(m)}; \\
0.8621 \cdot \left(w_6^{(u)} - w_7^{(l)}\right) \geq \zeta^{(u)}; \\
0.6757\left(w_7^{(u)}\right) \geq \zeta^{(l)}; 0.8065\left(w_7^{(m)}\right) \geq \zeta^{(m)}; 1.000\left(w_7^{(l)}\right) \geq \zeta^{(u)}; \\
\sum_{j=1}^{17} w_j^{(l)} = 0.8; \sum_{j=1}^{17} w_j^{(m)} = 1; \sum_{j=1}^{17} w_j^{(u)} = 1.2; \quad \forall_j; \\
w_j^{(l)}, w_j^{(m)}, w_j^{(u)} \geq 0; \quad \forall_j \\
w_j^{(l)} \leq w_j^{(m)} \leq w_j^{(u)}; \quad \forall_j
\end{cases}$$

Lingo 17.0 software was used to solve the model. The fuzzy weight coefficients of the criteria are shown in Fig. 25. In Fig. 25, it can be seen that the importance of criterion C2 dominates over other criteria, while criteria C14, C6, and C7 have the least importance in the decision-making model.

4.2.2. Fuzzy TRWA methodology

In the study, a set of seven alternatives was considered, which were ranked based on a defined set of seventeen criteria. The TRWA methodology was used for the evaluation, which is presented in the next part.

Step 1: The data based on which the alternatives were evaluated is presented in the initial decision matrix, Table 17.

Criteria C1–C11 represent quantitative criteria that are defined based on exact measurements, while C12–C17 represent qualitative criteria, and a fuzzy scale was used to represent them (see Table 15).

By applying Eq. (18), the elements of the initial decision matrix (see Table 17) were standardised, which are represented by different measurement units. By standardising the elements from Table 17, the transformation of the elements into the interval [0,1] was performed. The standardised initial decision matrix is given in Table 18.

Step 2: Using Eqs. (19) and (20), trigonometric fuzzy weighted strategy alternatives are defined (Fig. 26(a) and (b)). Based on Fig. 26(a)

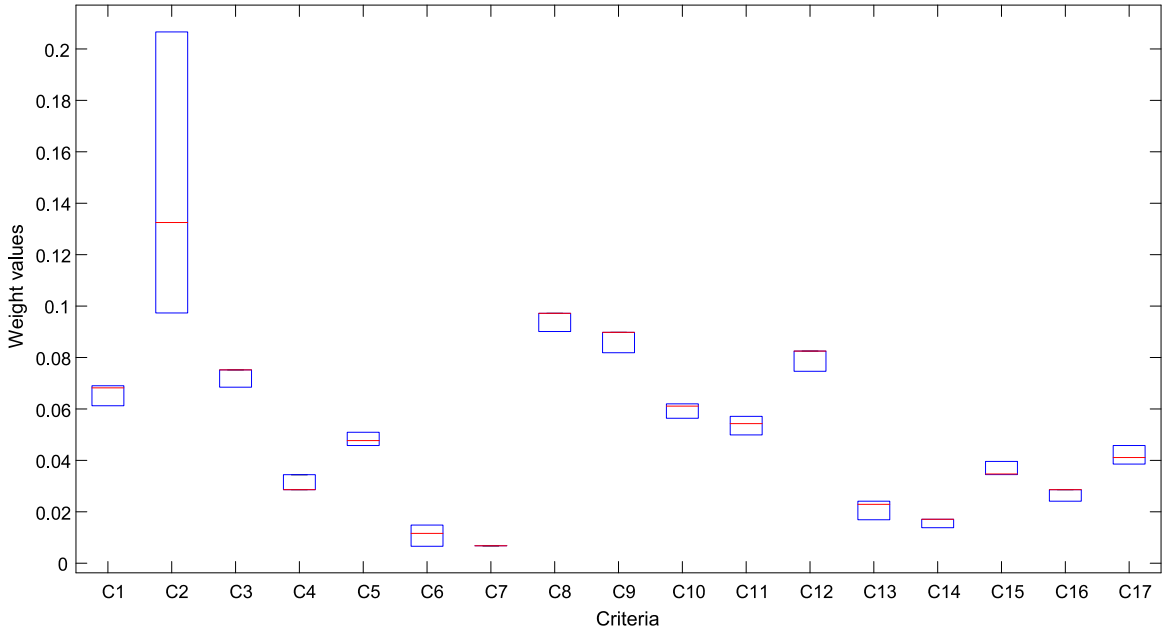

Fig. 25. Final fuzzy values of weighting coefficients.

Table 17
Initial decision matrix.

	A_1	A_2	A_3	A_4	A_5	A_6	A_7
C1	10.60	10.58	8.45	8.19	8.13	7.93	8.82
C2	3999.39	4143.38	3095.31	3082.32	2895.97	3175.45	3441.67
C3	48.06	49.79	37.19	37.04	34.80	38.16	41.36
C4	65.00	60.00	34.00	55.00	45.00	63.00	89.00
C5	235.00	234.00	18.00	20.00	37.00	23.00	54.00
C6	149.00	140.00	1.00	2.00	11.00	0.00	14.00
C7	2.10	2.00	0.60	1.80	2.00	0.80	2.10
C8	3.653	3.651	3.138	3.162	3.213	3.247	3.306
C9	90.17	90.15	80.13	83.87	86.51	80.79	83.60
C10	8.43	7.97	10.95	16.02	15.84	10.22	9.67
C11	2.12	2.10	0.41	0.42	0.54	0.46	0.65
C12	VH	VH	AH	AH	MH	MH	MH
C13	VL	MH	VL	VL	VL	VL	VL
C14	VL	VL	MH	VH	MH	MH	VH
C15	VL	AL	MH	MH	MH	MH	VL
C16	ML	ML	VH	MH	MH	MH	ML
C17	AH	AH	VL	VL	MH	MH	AH

Table 18
Standardised initial decision matrix.

	A_1	A_2	A_3	A_4	A_5	A_6	A_7
C1	1.000	0.998	0.797	0.773	0.767	0.748	0.832
C2	0.965	1.000	0.747	0.744	0.699	0.766	0.831
C3	0.965	1.000	0.747	0.744	0.699	0.766	0.831
C4	0.652	0.708	1.000	0.764	0.876	0.674	0.382
C5	0.077	0.081	1.000	0.991	0.919	0.979	0.847
C6	0.000	0.060	0.993	0.987	0.926	1.000	0.906
C7	0.286	0.333	1.000	0.429	0.333	0.905	0.286
C8	0.859	0.859	1.000	0.994	0.979	0.970	0.954
C9	0.885	0.885	0.960	0.955	0.925	1.000	0.958
C10	0.971	1.000	0.814	0.498	0.509	0.860	0.894
C11	0.193	0.203	1.000	0.995	0.939	0.976	0.887
C12	(0.75,0.85,0.95)	(0.75,0.85,0.95)	(0.85,0.90,1.00)	(0.85,0.9,1.00)	(0.55,0.65,0.75)	(0.55,0.65,0.75)	(0.55,0.65,0.75)
C13	(0.73,0.87,1.00)	(0.20,0.33,0.47)	(0.73,0.87,1.00)	(0.73,0.87,1.00)	(0.73,0.87,1.00)	(0.73,0.87,1.00)	(0.73,0.87,1.00)
C14	(0.79,0.89,1.00)	(0.79,0.89,1.00)	(0.37,0.47,0.58)	(0.16,0.26,0.37)	(0.37,0.47,0.58)	(0.37,0.47,0.58)	(0.16,0.26,0.37)
C15	(0.67,0.73,0.87)	(0.73,0.87,1.00)	(0.13,0.20,0.33)	(0.13,0.20,0.33)	(0.13,0.20,0.33)	(0.13,0.20,0.33)	(0.67,0.73,0.87)
C16	(0.79,0.89,1.00)	(0.79,0.89,1.00)	(0.37,0.47,0.58)	(0.58,0.68,0.79)	(0.58,0.68,0.79)	(0.58,0.68,0.79)	(0.79,0.89,1.00)
C17	(0.85,0.90,1.00)	(0.85,0.90,1.00)	(0.15,0.25,0.35)	(0.15,0.25,0.35)	(0.55,0.65,0.75)	(0.55,0.65,0.75)	(0.85,0.90,1.00)

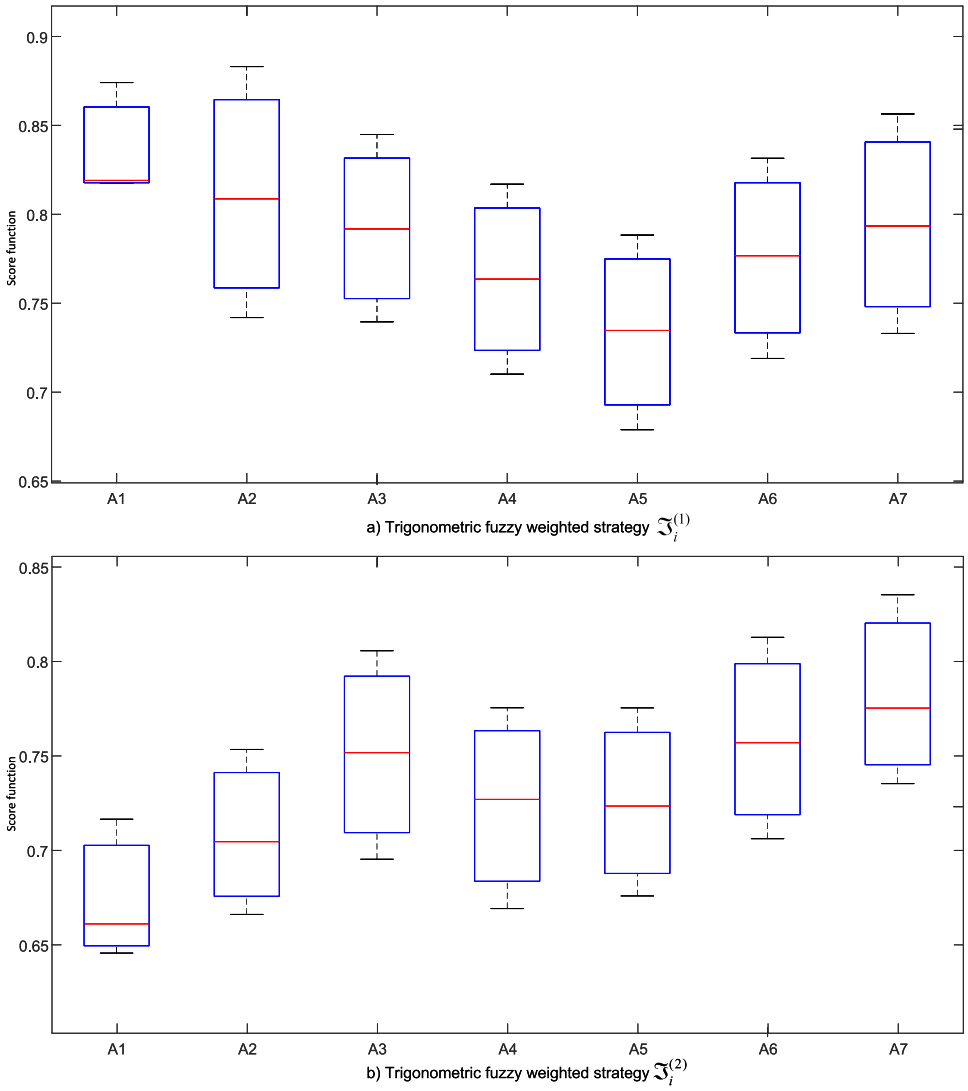

Fig. 26. Trigonometric fuzzy weighted strategies.

and (b), the values of $\mathfrak{F}_i^{(1)}$ and $\mathfrak{F}_i^{(2)}$, it is observed that alternatives A_7, A_6, and A_3 dominate the considered set of alternatives. Therefore, it is expected that they will maintain their dominance when defining the final score functions of the alternatives.

Step 3: Trigonometric fuzzy weighted strategies of alternatives were used to define the final rank of alternatives $\mathfrak{F}_i^{(1)}$ and $\mathfrak{F}_i^{(2)}$ were used to calculate the integrated score functions of alternatives using Eq. (21). For the calculation of integrated score functions, parameter values $\zeta = 0.5$, and $\delta = 1$ were adopted. Adopted parameter values simulate the equal influence of both trigonometric fuzzy weighted strategies on the final results and facilitate the calculation procedure of integrated score functions:

$$\nabla_i = \begin{matrix} A_1 \\ A_2 \\ A_3 \\ A_4 \\ A_5 \\ A_6 \\ A_7 \end{matrix} \begin{bmatrix} (0.714, 0.775, 0.805) \\ (0.696, 0.799, 0.796) \\ (0.726, 0.838, 0.824) \\ (0.690, 0.800, 0.790) \\ (0.680, 0.785, 0.774) \\ (0.718, 0.828, 0.816) \\ (0.750, 0.856, 0.845) \end{bmatrix},$$

where ∇_i denotes final assessment score of the alternatives.

The integrated score function of the alternatives is visually represented in Fig. 27, with score values also tabulated in Table 19. It is evident that alternative A_7 predominates over the others. Following this, A_3 emerges as the next most viable alternative, while A_1 and A_4 present as less favourable options. Analysing the derived values leads us to conclude that A_7 ranks highest, followed by A_3 and A_6, establishing the ranking as $\boldsymbol{A_7 > A_3 > A_6 > A_2 > A_4 > A_5 > A_1}$.

Table 19
The ranking of alternatives.

Alternatives	Score values	Rank
A_1	0.755	7
A_2	0.773	4
A_3	0.806	2
A_4	0.770	5
A_5	0.756	6
A_6	0.798	3
A_7	0.827	1

5. Discussion

The Discussion is organised into two main sections: Firstly, a critical examination of the resulting rankings of the alternatives is presented. Subsequently, a holistic discussion in the context of offshore energy is provided based on the site rankings.

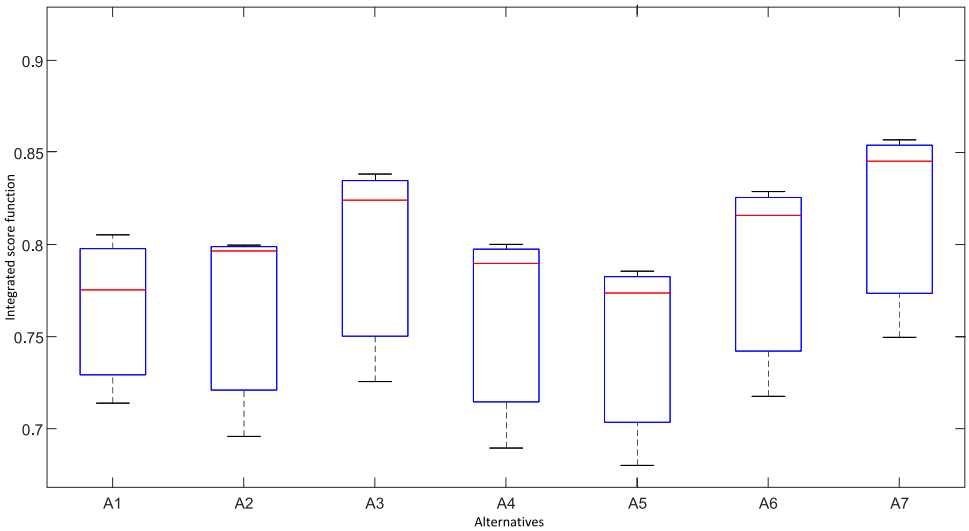

Fig. 27. Integrated score functions.

5.1. Sensitivity analysis and stability of the ranking results

In this section, a robustness check and sensitivity analysis of the initial solution was performed. In the literature, there is no uniform methodology to check the robustness of solutions in multicriteria problems. However, most authors believe that the sensitivity analysis and the robustness check of the solution should include the variation of the subjectively defined input parameters and the check of their influence on the initial results (Pala, 2022; Paul et al., 2022; Riaz and Farid, 2022). Two stabilisation parameters are used in the fuzzy TRWA model to generate integrated score functions. Therefore, in the following part, the analysed sensitivity of the initial solution in case of variation of parameters ζ and δ is presented.

5.1.1. The influence of the parameter ζ on the ranking results

The parameter ζ was used to define the influence of strategies $\mathfrak{F}_i^{(1)}$ and $\mathfrak{F}_i^{(2)}$ in the aggregation function Eq. (21). In the initial solution, the value $\zeta = 0.5$ was adopted. Since the parameter ζ takes values from the interval $\zeta \in [0, 1]$, its change through 49 scenarios is simulated in the following part. In the first scenario, the value $\zeta \approx 0.0$ was adopted, while in each subsequent scenario, the value was increased by 0.02. Fig. 28 shows the variations in the ranks of the alternatives during the simulation.

The results in Fig. 28 show that changing the parameter $0 \leq \zeta \leq 1$ leads to changes in the ranks of the alternatives. Changes in ranks result from different values of trigonometric fuzzy-weighted strategy alternatives (see Fig. 26). It is evident that there are differences in the initial ranks within fuzzy weighted strategies, so these differences cause changes in the ranks when the parameter ζ is varied. Despite the changes in the ζ parameter, the A_7 alternative maintained its dominance through all scenarios. Also, alternatives A_3 and A_6 proved to be good enough alternative solutions. In order to assess the statistical significance of changes in ranks, a correlation check was performed between the initial solution and the changes shown during the scenario. Fig. 29 shows the statistical correlation using Spriman's correlation coefficient.

The statistical correlation coefficient (see Fig. 29) ranges in the interval $[0.878, 1]$, which confirms the high correlation between the results obtained during the simulation. Also, the results demonstrate that alternative A_7 dominates the other alternatives and represents the best solution.

5.1.2. The influence of the parameter δ on the ranking results

In this part, the change of the parameter δ was simulated in the interval $1 \leq \delta \leq 50$. Fig. 30 shows the changes in the score functions of alternatives A_1 and A_2, which occurred due to the change in the parameter δ. Similar changes occur with the remaining alternatives.

The changes in the score functions of the alternatives, shown in Fig. 30(a) and (b), confirm the dependence of the results on the value of the parameter δ. In order to compare the dependence of the results, Fig. 31 shows the intervals in the square where the variations of the score functions occur.

The results in Figs. 30(a)–(b) and 31 indicate that the score functions of the initial solution depend on the adopted value of the parameter δ. However, since these variations occur in a small criterion interval, these changes cause small shifts in the score functions of the alternatives (see Fig. 31). This is also confirmed by the statistical correlation coefficient that was considered for the results obtained during the simulation. The statistical correlation is in the interval $[0.925, 1]$, which confirms the results in Fig. 31. Therefore, based on the presented simulation, it was confirmed that the initial ranking is credible and that alternative A_7 represents the best solution within the considered set.

5.2. A holistic evaluation within the context of offshore wind energy

Businesses and governments targeting the development of offshore wind projects should select their investment locations with great care. These substantial energy expenditures are meticulously planned over months or even years due to the large-scale nature of offshore wind energy projects, which necessitates the mobilisation of billions of euros. The decision-making process aims to prove the most optimal investment choice and is grounded in a spectrum of analyses and research. This process is intricate and deals with a myriad of technical, economic, financial, environmental, and political issues.

An expansive set of quantitative and qualitative metrics is employed to establish a multidisciplinary criterion set. It is vital that these systems encapsulate the insights of various experts to feed a well-designed decision-making algorithm or mechanism effectively.

5.2.1. Techno-economic perspective

Wind speed values, which are easily accessible with minimal effort, are essential data for potential wind energy projects and their respective locations. Investors can quickly evaluate and classify locations based solely on wind speed data. In such a scenario, the selected locations for the offshore wind farm might be arranged in this order: $A_1 > A_2 > A_7 > A_3 > A_4 > A_5 > A_6$ (Sørlige Nordsjø I >

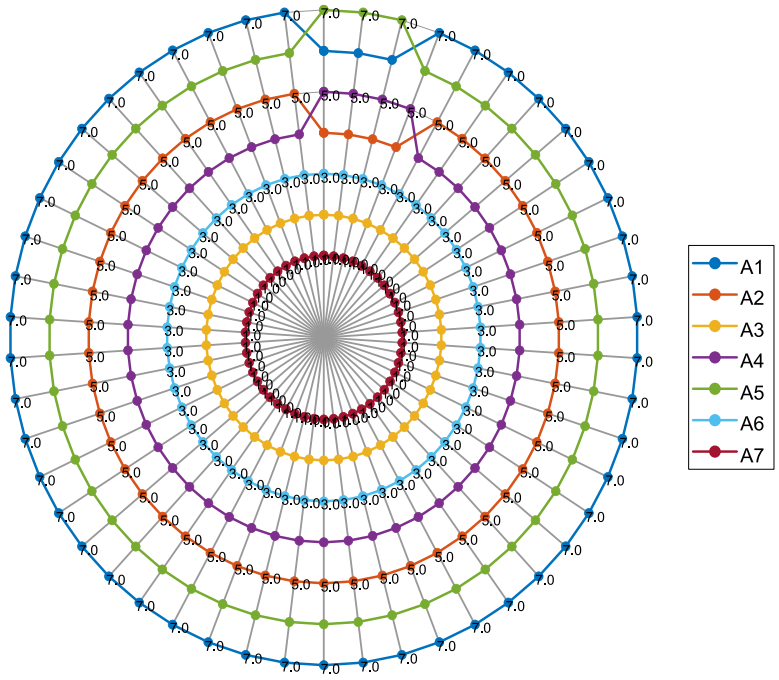

Fig. 28. Variations in the ranks of the alternatives during the scenario.

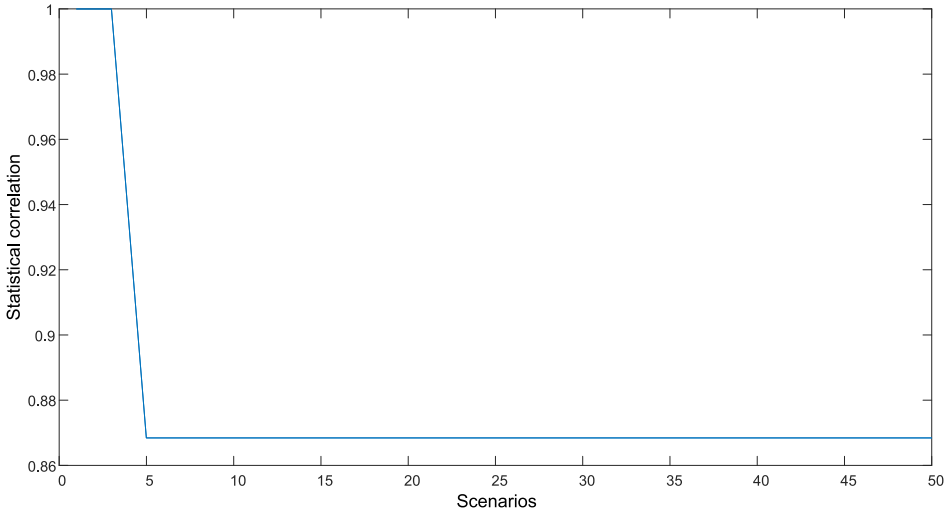

Fig. 29. Statistical correlation of ranks.

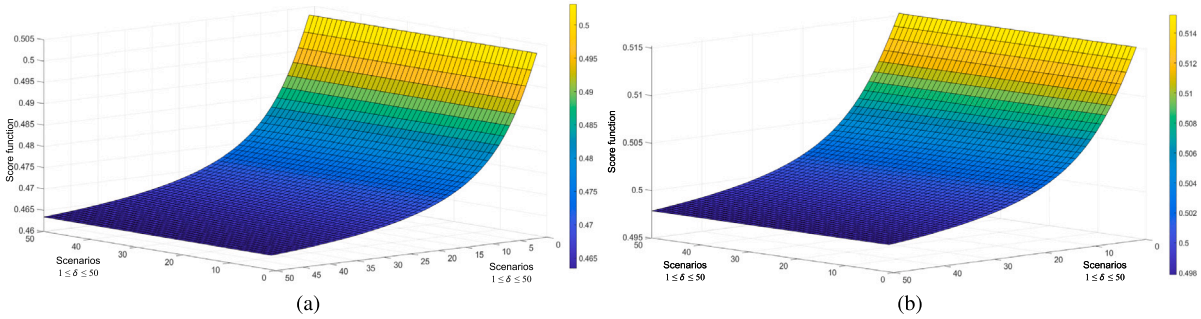

Fig. 30. Parameter δ: Change of score functions of (a) Alternative A_1, and (b) Alternative A_2.

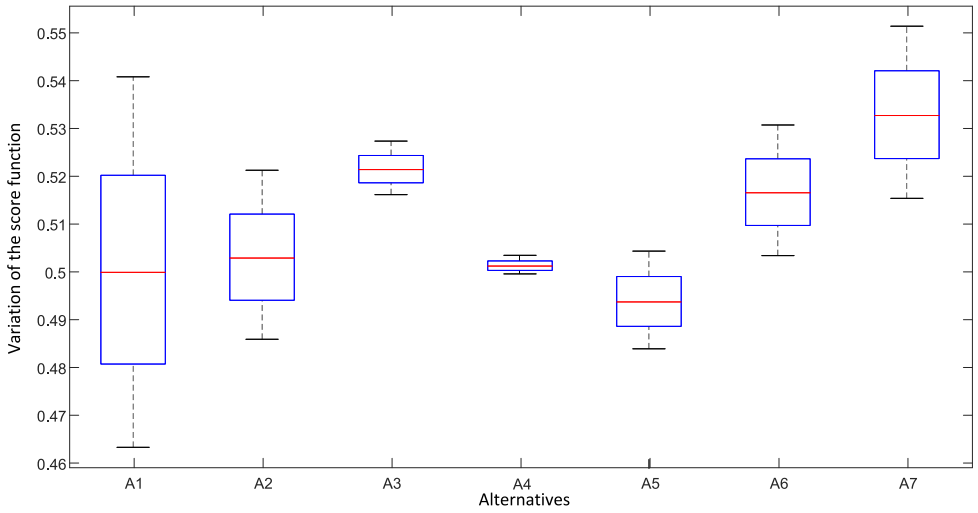

Fig. 31. Parameter δ: Variations of the integrated score functions of all alternatives.

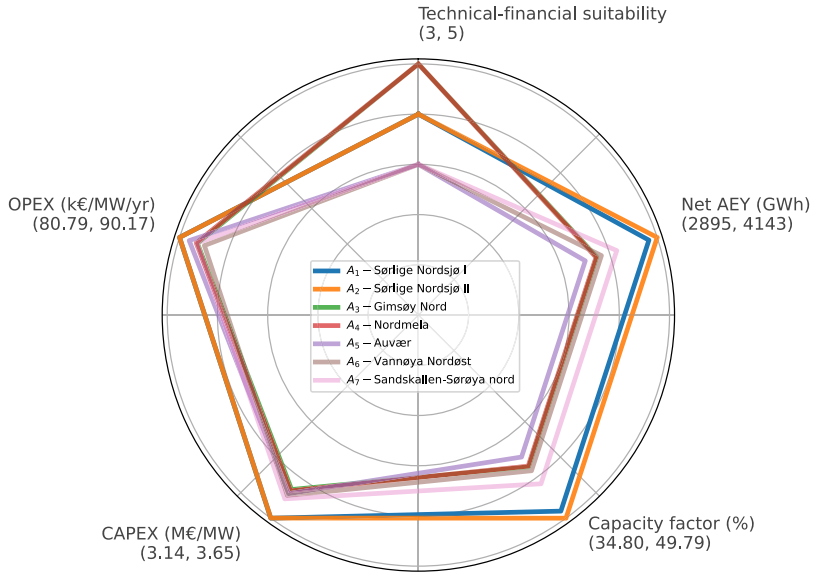

Fig. 32. Criteria with the highest weights vs. site locations.

Sørlige Nordsjø II > Sandskallen-Sørøya Nord > ⋯ > Auvær > Vannøya Nordøst).

However, if the investor's decision-makers also consider other significant criteria, such as the capacity factor, when ranking the investment alternatives, the arrangement could differ as in the following: $A_2 > A_1 > A_7 > A_6 > A_3 > A_4 > A_5$ (Sørlige Nordsjø II > Sørlige Nordsjø I > ⋯ > Nordmela > Auvær). For an initial, straightforward comparison, the top five highly ranked criteria, according to the expert assessments displayed in Table 16, are illustrated in a spider plot in Fig. 32.

The decision-making algorithm proposed in this work suggested the following order of sites that are significantly different from those first-hand rankings above: $A_7 > A_3 > A_6 > A_2 > A_4 > A_5 > A_1$. Detailed elaboration on the results reveals more in-depth insights. According to the outputs of the decision-making algorithm, A_7 (Sandskallen-Sørøya Nord) emerges as the most favourable investment priority when all sets of criteria are taken into account. However, if the decision were to be guided solely by the mean wind speed, net AEY, and CF, A_1 (Sørlige Nordsjø I) and A_2 (Sørlige Nordsjø II) would be the optimal choices. The sites A_2 (Sørlige Nordsjø II) and A_1 (Sørlige Nordsjø I) became significantly less favourable when more nuanced, multidisciplinary factors such as CAPEX, OPEX, distance to coast, distance to the grid connection point, and export cable length were considered.

The second best option appears to be A_3 (Gimsøy Nord), as also shown in Table 19. Although it holds the fourth-best mean wind speed and fifth-best net AEY and CF, it stands at the top position in terms of distance to the shore and distance to the grid connection point, which affects the export cable length, consequently leading to the lowest electrical losses and CAPEX among all sites. Gimsøy Nord was also given the highest techno-economic suitability grade in the NVE report in terms of technical-financial suitability (Berg et al., 2012).

A_6 (Vannøyya Nordøst) has the lowest wind speed, fourth-highest CF and AEY, CAPEX, the third-longest distance to the grid connection, and the lowest OPEX. These comprehensive criteria results enable A_6 (Vannøyya Nordøst) to get the third-best position overall.

5.2.2. *Environmental and social perspectives*

The elucidated results emphasise a spectrum of suitability and environmental impact across the sites. While sites like Gimsøy Nord and Nordmela stand out in terms of technical-financial feasibility, they also exhibit significant environmental impacts across various criteria, such as fisheries, marine species, and sea birds. On the other hand, Sørlige

Nordsjø I and Sørlige Nordsjø II demonstrate more balanced profiles, showcasing high technical-financial suitability and the lowest environmental impacts. Sandskallen-Sørøya Nord demonstrated the third-best balanced profile among all, according to NVE's criteria.

Given the criteria and additional quantitative data explored in Drivenes et al. (2010), Berg et al. (2012) and Multiconsult (2012), NVE has recommended that Sørlige Nordsjø I, Sørlige Nordsjø II, and Sandskallen-Sørøya Nord should receive the highest legislative focus, spotlighting these sites as potential focal points of interest or priority for governmental bodies or policies. It is important to note that Sørlige Nordsjø I and II are mutually exclusive areas, implying that selecting one automatically negates the other.

5.2.3. Limitations and outlook

The Norwegian Water Resources and Energy Directorate, NVE, holds the principal responsibility in Norway concerning energy-related affairs, encompassing offshore energy projects and investments. Consequently, it is important that the results of this study are aligned with the findings and viewpoints of NVE. After an overall assessment, NVE recommended prioritising the opening of the areas Sørlige Nordsjø II, Utsira Nord (not covered in this work), Frøyagrunnene (not covered in this work), and Sandskallen-Sørøya Nord in the first half (Category A) where Category A is the most attractive (NVE, 2017). As mentioned in Section 3.2, on 12th June 2020, the government decided to open Utsira Nord and Sørlige NordsjøII for offshore renewable energy production and that the power from the first phase of Sørlige Nordsjø II (1500 MW) will be sent to the Norwegian mainland (Ministry of Petroleum and Energy, 2021). The announcement of the first phase of Sørlige Nordsjø II and Utsira Nord is planned for the first quarter of 2023, with the subsequent allocation of the areas during the year. NVE reported that these areas stood out as areas with very good technical-economic conditions, and those overall consequences were assessed as acceptable.

On the contrary, our decision-making framework suggested that Sørlige Nordsjø II is the fourth-best site, while Sørlige Nordsjø I is ranked last. These results seem to somewhat disagree with NVE's priorities. The primary reason for this discrepancy is that the maximum power capacity of each site was a factor in NVE's evaluation criteria, while a uniform power capacity (950 MW) was applied to each site in this work. In consideration of future developments, our offshore wind farm layout consisting of a 10 × 10 configuration of wind turbines has been used as a demonstrative model, providing insight into the customisable nature of offshore energy systems. The stated capabilities for offshore locations provide potential for future growth and development. To elaborate, Sørlige Nordsjø I and II have an estimated capacity of 1000 MW, while the remaining sites are each estimated to have a capacity of 200 MW (Drivenes et al., 2010; Berg et al., 2012). The approach by Multiconsult (2012), upon which the Berg et al. (2012) report was largely predicated, significantly favoured Sørlige Nordsjø I and II due to their five-fold greater capacity, which can enable enhanced production in the coming years despite their notably higher CAPEX and OPEX costs. Although the report acknowledged that far offshore installations, being considerably more exposed to intensive weather conditions, would likely incur higher O&M costs per MW (i.e., OPEX), this was not detailed in the calculations. Additionally, substantially increased investments in the HVDC conversion station or investments for reactive power compensation if HVAC was chosen over HVDC, thicker/longer export cables, foundation costs, and so forth, which significantly elevate the total CAPEX, were not accorded sufficient weight. Instead, the focus was placed on how these far-offshore zones of 1000 MW would allow for economies of scale compared to the 200 MW zones. We believe that NVE's approach notably favoured Sørlige Nordsjø I and II over the 200-MW capacity zones in terms of the LCOE in their model, creating significant economic attractiveness despite the increased technical and environmental challenges, as well as underestimated CAPEX and OPEX calculations. For instance, in our model, the electrical losses with and without reactive power compensation differ around 5.6% and 5.4% for Sørlige Nordsjø I and II, respectively. This discrepancy amounts to a 227 GWh difference in the net AEY, which translates to an annual financial impact of 28.3 M€, based on the 2nd quarter of 2023 electricity prices in Norway (Statistics Norway, 2023). As illustrated, even minor variations in the depth of cost calculations can lead to substantial discrepancies in cost predictions, particularly since the differences between sites are not markedly significant and such variations can readily influence the ranking.

In order to modify and improve the decision-making process over time, it will be necessary to conduct further research and maintain a constant monitoring of legislation, technical improvements, and environmental issues. The accuracy of the suggested model could be increased by increasing the number of researchers with more varied backgrounds from different disciplines. The proposed approach is anticipated to be used as a form of reference material by academics, commercial businesses who are interested in making such investments, and decision-makers. Moreover, despite the thoroughness of the electrical loss model covered in this paper, it did not include a detailed power systems analysis to calculate power losses or associated costs, which will be addressed in a follow-up study.

Finally, our research highlights the significance of offshore energy, particularly against the backdrop of the ever-changing global energy landscape, which includes but is not limited to, the current war in Ukraine. Norway can undoubtedly contribute to the energy supply safety of its European neighbours by exporting surplus energy, especially from offshore wind energy resources, should public opinion support this option. With its substantial offshore reserves, Norway is well-positioned to play a pivotal role in advancing European energy independence and aiding the development of a more secure and robust energy framework across the continent. Moreover, there is notable potential for establishing a more expansive offshore power network, especially in southern Norway, which could enhance energy partnerships between nations. Further possibilities and scenarios in the field of offshore wind generation require continuous investigation and strategic planning.

6. Conclusion

The primary objective of this study was to develop a novel multi-criteria decision-making framework specifically tailored to address the multifaceted challenges inherent in OWF siting, demonstrated through a strategic case study ranking potential offshore wind farm locations in Norway. To that end, we introduced a two-stage fuzzy mathematical model, which integrates the Ordinal Priority Approach, F-OPA, and non-linear sine trigonometric functions, TRWA, all underpinned by a thorough techno-economic assessment. This involved generating power loss estimations employing a specialised reactive power compensation model tailored for OWFs and executing energy economic calculations to reinforce our decision-making framework.

The TRWA model, which enables the incorporation of diverse factors in determining the most suitable locations for OWF projects, is the foundation for the decision-making algorithm. Using this approach, we were able to evaluate the benefits and drawbacks of the different solutions and rank them according to their total performance ratings. The stability of the model was affirmed through a sensitivity analysis, wherein the statistical correlation coefficient was within the intervals [0.878, 1] and [0.925, 1] in two distinct analyses. One of the limitations of the TRWA model is the inability to identify and eliminate extreme and unreasonable elements in the initial decision matrix. This limitation can successfully be eliminated by integrating power averaging functions into the TRWA algorithm, which can be one of the directions for future research. Also, it is necessary to emphasise that the fuzzy TRWA model cannot process information that is presented using neutral and false elements. Therefore, in future research, it is essential to consider the possibility of applying intuitionistic fuzzy, neutrosophic or picture fuzzy sets in the TRWA model.

The comprehensive criteria chosen in this work included wind speed, net annual energy yield, capacity factor, as well as considerations pertaining to technology, economics, energy policy, and the environment. The algorithm output ranked the sites from best to worst as follows: Sandskallen-Sørøya Nord, Gimsøy Nord, Vannøya Nordøst, Sørlige Nordsjø II, Nordmela, Auvær, and finally, Sørlige Nordsjø I. However, were the decision based solely on quantitative parameters such as the mean wind speed, net annual energy yield, and capacity factor, Sørlige Nordsjø I and Sørlige Nordsjø II would emerge as the optimal choices. Yet, when more detailed, multidisciplinary considerations were factored in – including reactive power compensation, tailored CAPEX, OPEX, distance to the coast, proximity to the grid connection point, and length/size of export cable – the attractiveness of sites Sørlige Nordsjø I and Sørlige Nordsjø II significantly diminished. To elaborate, our integrated power loss and reactive power compensation model revealed a 227 GWh variation in the net AEY between the sites Sørlige Nordsjø I and II, equating to an annual financial impact of 28.3 M€, based on the 2nd quarter of 2023 electricity prices in Norway. Evidently, even slight nuances in the detail level of cost calculations can substantially skew cost estimates and influence site ranking, particularly when inter-site differences are subtle.

Our decision-making framework showed a notable divergence from NVE's approach in ranking Sørlige Nordsjø II and I, primarily due to our focused consideration of site power capacities and comprehensive economic assessments. While NVE's preference for Sørlige Nordsjø I and II was largely based on the five-fold larger power capacity of those sites, our analysis implemented a uniform power capacity for all sites. As our model showed, more detailed CAPEX, OPEX, and power loss calculations, as well as increased accuracy in the model, can potentially offset the advantages offered by economies of scale in larger power zones and influence site ranking.

CRediT authorship contribution statement

Umit Cali: Conceptualization, Data curation, Methodology, Project administration, Supervision, Validation, Visualization, Writing – original draft, Writing – review & editing. **Emre Kantar:** Conceptualization, Data curation, Formal analysis, Investigation, Methodology, Project administration, Resources, Validation, Visualization, Writing – original draft, Writing – review & editing. **Dragan Pamucar:** Methodology, Software, Validation, Writing – original draft, Writing – review & editing. **Muhammet Deveci:** Conceptualization, Data curation, Software, Visualization, Writing – original draft, Writing – review & editing. **Peter Taylor:** Data curation, Methodology, Writing – original draft, Writing – review & editing. **David Campos-Gaona:** Data curation, Methodology, Writing – original draft, Writing – review & editing. **Olimpo Anaya-Lara:** Project administration, Writing – original draft. **John O. Tande:** Funding acquisition, Project administration, Supervision, Writing – original draft, Writing – review & editing.

Declaration of competing interest

The authors declare that they have no known competing financial interests or personal relationships that could have appeared to influence the work reported in this paper.

Data availability

Data will be made available on request.

Acknowledgements

This work has been partially supported by the Norwegian Research Centre on Wind Energy (NorthWind). NorthWind (2021–2029) is a Centre for Environmental-Friendly Energy Research co-financed by the Research Council of Norway (contract 321954).

References

Abdel-Basset, M., Gamal, A., Chakrabortty, R.K., Ryan, M., 2021. A new hybrid multi-criteria decision-making approach for location selection of sustainable offshore wind energy stations: A case study. J. Clean. Prod. 280, 124462. http://dx.doi.org/10.1016/j.jclepro.2020.124462.

Adedeji, P.A., Akinlabi, S.A., Madushele, N., Olatunji, O.O., 2020. Neuro-fuzzy resource forecast in site suitability assessment for wind and solar energy: A mini review. J. Clean. Prod. 269, 122104. http://dx.doi.org/10.1016/j.jclepro.2020.122104.

Ataei, Y., Mahmoudi, A., Feylizadeh, M.R., Li, D.-F., 2020. Ordinal priority approach (OPA) in multiple attribute decision-making. Appl. Soft Comput. 86, 105893. http://dx.doi.org/10.1016/j.asoc.2019.105893.

Baptista, J., Lima, F., Cerveira, A., 2021. Optimization of wind turbines placement in offshore wind farms: Wake effects concerns. Commun. Comput. Inf. Sci. 1488 CCIS, 102–109. http://dx.doi.org/10.1007/978-3-030-91885-9_8.

Beiter, P., Musial, W., Smith, A., Kilcher, L., Damiani, R., Maness, M., Sirnivas, S., Stehly, T., Gevorgian, V., Mooney, M., Scott, G., 2016. A Spatial-Economic Cost-Reduction Pathway Analysis for U.S. Offshore Wind Energy Development from 2015–2030. Technical Report NREL/TP-6A20-66579, National Renewable Energy Lab. (NREL), Golden, CO (United States), http://dx.doi.org/10.2172/1324526.

Berg, K.S., Carlsen, M., Eirum, T., Jakobsen, S.B., Johnson, N.H., Mindeberg, S.K., Nybakke, K., Sydness, G.S., 2012. Havvind. Strategisk Konsekvensutredning. Technical Report, The Norwegian Water Resources and Energy Directorate (NVE), URL: https://publikasjoner.nve.no/rapport/2012/rapport2012_47.pdf.

Beuckelaers, W., 2017. Numerical Modelling of Laterally Loaded Piles for Offshore Wind Turbines (Ph.D. thesis). University of Oxford, URL: https://ora.ox.ac.uk/objects/uuid:9feba16c-fc8e-464e-8928-3ca3a7a9fb73.

Bjerkseter, C., Ågotnes, A., 2013. Levelised Costs of Energy for Offshore Floating Wind Turbine Concepts (Master's thesis). Norwegian University of Life Sciences, Ås, URL: https://nmbu.brage.unit.no/nmbu-xmlui/bitstream/handle/11250/189073/Bjerkseter,%20C.%20&%20%C3%85gotnes,%20A.%20(2013)%20-%20Levelised%20Costs%20of%20Energy%20for%20Offshore%20Floating%20Wind%20Turbine%20Concepts.pdf?sequence=1.

BloombergNEF, 2022. Wind turbine price index. https://data.bloomberglp.com/bnef/sites/24/2022/03/Wind-Turbine-Price-Index-March-2022.pdf.

Bonab, S.R., Haseli, G., Rajabzadeh, H., Ghoushchi, S.J., Hajiaghaei-Keshteli, M., Tomaskova, H., 2023. Sustainable resilient supplier selection for IoT implementation based on the integrated BWM and TRUST under spherical fuzzy sets. Decis. Mak.: Appl. Manag. Eng. 6 (1), 153–185. http://dx.doi.org/10.31181/dmame12012023b.

Borrmann, R., Rehfeld, K., Wallasch, A.-K., Lüers, S., 2018. Capacity Densities of European Offshore Wind Farms. Technical Report, Deutsche WindGuard GmbH, p. 83, URL: https://vasab.org/wp-content/uploads/2018/06/BalticLINes_CapacityDensityStudy_June2018-1.pdf.

Dağıstanlı, H.A., 2023. An integrated fuzzy MCDM and trend analysis approach for financial performance evaluation of energy companies in borsa Istanbul sustainability index. J. Soft Comput. Decis. Anal. 1 (1), 39–49. http://dx.doi.org/10.31181/jscda1120233.

Dakic, J., Cheah-Mane, M., Gomis-Bellmunt, O., Prieto-Araujo, E., 2021. HVAC transmission system for offshore wind power plants including mid-cable reactive power compensation: Optimal design and comparison to VSC-HVDC transmission. IEEE Trans. Power Deliv. 36 (5), 2814–2824. http://dx.doi.org/10.1109/TPWRD.2020.3027356.

Deveci, M., Pamucar, D., Cali, U., Kantar, E., Kölle, K., Tande, J.O., 2022. Hybrid q-rung orthopair fuzzy sets based CoCoSo model for floating offshore wind farm site selection in Norway. CSEE J. Power Energy Syst. 8 (5), 1261–1280. http://dx.doi.org/10.17775/CSEEJPES.2021.07700.

Dicorato, M., Forte, G., Pisani, M., Trovato, M., 2011. Guidelines for assessment of investment cost for offshore wind generation. Renew. Energy 36 (8), 2043–2051. http://dx.doi.org/10.1016/j.renene.2011.01.003.

Dinçer, H., Yüksel, S., Eti, S., 2023. Identifying the right policies for increasing the efficiency of the renewable energy transition with a novel fuzzy decision-making model. J. Soft Comput. Decis. Anal. 1 (1), 50–62. http://dx.doi.org/10.31181/jscda1120234.

DNV, 2023. Offshore wind 2023: New ambitions, new challenges. URL: https://www.dnv.com/article/offshore-wind-2023-new-ambitions-new-challenges--243462. Accessed: 2023-07-05.

DOE, 2020. Wind Energy Technologies Office 2020 Research Portfolio. Technical Report, U.S. Department of Energy, URL: https://www.energy.gov/eere/wind/downloads/2020-wind-energy-technologies-office-research-portfolio.

Drivenes, A.F., Eirum, T.N., Johnson, N.H.N., Mindeberg, S.K.N., Lunde, S.K., Undem, L.S.N., Veggeland, K.O., Veie-Rosvoll, B.D., Voksø, A.N., 2010. Havvind - Forslag Til Utredningsområder. Technical Report, regjeringen.no, URL: https://www.regjeringen.no/no/dokumenter/havvind---forslag-til-utredningsomrader/id620670/.

Technical University of Denmark (DTU), 2023. Global wind atlas. URL: https://globalwindatlas.info/en. Available online, Accessed: 2023-10-12.

Dupont, E., Koppelaar, R., Jeanmart, H., 2018. Global available wind energy with physical and energy return on investment constraints. Appl. Energy 209, 322–338. http://dx.doi.org/10.1016/j.apenergy.2017.09.085.

ENTSO-e, 2011. Offshore Transmission Technology. Report, European Network of Transmission System Operators for Electricity, URL: https://www.entsoe.eu/fileadmin/user_upload/_library/publications/entsoe/SDC/European_offshore_grid_-_Offshore_Technology_-_FINALversion.pdf.

ESO, N.G., 2013. Electricity Ten Year Statement. Report, National Grid ESO, URL: https://www.nationalgrideso.com/document/46916/download.

Global Modeling and Assimilation Office, 2023. MERRA-2. URL: https://gmao.gsfc.nasa.gov/reanalysis/MERRA-2/. [Online; accessed 28-September-2023].

Gökalp, Y., Dinçer, H., Eti, S., Yüksel, S., 2024. Generating a novel artificial intelligence-based decision-making model for determining priority strategies for improving community health. Journal of Operations Intelligence 2 (1), 1–13. http://dx.doi.org/10.31181/jopi21202413.

Guiping, Z., Xiaowei, D., Chen, Z., 2015. Optimisation of reactive power compensation of HVAC cable in off-shore wind power plant. IET Renew. Power Gener. 9 (7), 857–863. http://dx.doi.org/10.1049/iet-rpg.2014.0375.

Hu, X., Pedrycz, W., Wang, X., 2015. Comparative analysis of logic operators: a perspective of statistical testing and granular computing. Internat. J. Approx. Reason. 66, 73–90. http://dx.doi.org/10.1016/j.ijar.2015.07.011.

IEC, 2012. BS IEC 60287-3-2:2012. Technical Report, International Electrotechnical Commission (IEC).

IRENA, 2020. Renewable Power Generation Costs in 2019. Technical Report, International Renewable Energy Agency (IRENA), URL: https://www.irena.org/publications/2020/Jun/Renewable-Power-Costs-in-2019.

IRENA, 2021. Renewable Capacity Statistics 2021. Technical Report, International Renewable Energy Agency (IRENA), URL: https://www.irena.org/publications/2021/Apr/Renewable-Capacity-Statistics-2021.

Kheirabadi, A.C., Nagamune, R., 2019. A quantitative review of wind farm control with the objective of wind farm power maximization. J. Wind Eng. Ind. Aerodyn. 192, 45–73. http://dx.doi.org/10.1016/j.jweia.2019.06.015.

Krishankumar, R., Nimmagadda, S.S., Rani, P., Mishra, A.R., Ravichandran, K., Gandomi, A.H., 2021. Solving renewable energy source selection problems using a q-rung orthopair fuzzy-based integrated decision-making approach. J. Clean. Prod. 279, 123329. http://dx.doi.org/10.1016/j.jclepro.2020.123329.

Langeland, M., Veim, A.K., 2012. Fagrapport Til Strategisk Konsekvensutredning Av Fornybar Energiproduksjon Til Havs – Fiskeriinteresser. Technical Report, Fiskeridirektoratet, URL: http://hdl.handle.net/11250/131799.

Lazard, 2020. Lazard's Levelized Cost of Energy Analysis - Version 14.0. Technical Report, Lazard, URL: https://www.lazard.com/perspective/levelized-cost-of-energy-and-levelized-cost-of-storage-2020/.

Li, M., Jiang, X., Carroll, J., Negenborn, R.R., 2022. A multi-objective maintenance strategy optimization framework for offshore wind farms considering uncertainty. Appl. Energy 321, 119284. http://dx.doi.org/10.1016/j.apenergy.2022.119284.

LS Cable, 2008. EHV Cable System 66 500kV XLPE Cable & Accessories. Technical Report, LS Cable & System, URL: https://www.powerandcables.com/wp-content/uploads/2017/12/LS-Cable-HV-EHV-XLPE-Cables-Joints-Systems-66kV-500kV.pdf.

Lundberg, S., 2003. Performance Comparison of Wind Park Configurations. Technical Report NREL/TP-6A20-66579, Department of Electric Power Engineering School of Electrical Engineering, Chalmers University of Technology, URL: https://www.osti.gov/etdeweb/servlets/purl/20437701.

Maienza, C., Avossa, A., Ricciardelli, F., Coiro, D., Troise, G., Georgakis, C.T., 2020. A life cycle cost model for floating offshore wind farms. Appl. Energy 266, 114716. http://dx.doi.org/10.1016/j.apenergy.2020.114716.

Ministry of Petroleum and Energy, 2021. Vindkraft til havs - tidslinje. URL: https://www.regjeringen.no/no/tema/energi/vindkraft-til-havs/id2873850/#:~:text=Omr%C3%A5dene%20Utsira%20Nord%20og%20S%C3%B8rlige,sendes%20til%20det%20norske%20fastlandet.

Mukhametzyanov, I., 2023. On the conformity of scales of multidimensional normalization: An application for the problems of decision making. Decis. Mak.: Appl. Manag. Eng. 6 (1), http://dx.doi.org/10.31181/dmame05012023i, 399–431.

Multiconsult, 2012. Fagrapport til strategisk konsekvensutredning av fornybar energiproduksjon til havs – teknologiog kostnadsutvikling.

Norwegian Government, 2023. Norway's new climate target: Emissions to be cut by at least 55%. URL: https://www.regjeringen.no/en/aktuelt/norways-new-climate-target-emissions-to-be-cut-by-at-least-55-/id2944876/. Accessed: 2023-06-28.

NVE, The Norwegian Water Resources and Energy Directorate (NVE), 2017. Svar på oppdrag om åpning av områder for vindkraft til havs.

Opricovic, S., Tzeng, G.-H., 2004. Compromise solution by MCDM methods: A comparative analysis of VIKOR and TOPSIS. European J. Oper. Res. 156 (2), 445–455. http://dx.doi.org/10.1016/j.ijar.2015.07.011.

Pala, O., 2022. A mixed-integer linear programming model for aggregating multi–criteria decision making methods. Decis. Mak.: Appl. Manag. Eng. 5 (2), 260–286. http://dx.doi.org/10.31181/dmame0318062022p.

Pamučar, D., Ćirović, G., 2015. The selection of transport and handling resources in logistics centers using multi-attributive border approximation area comparison (MABAC). Expert Syst. Appl. 42 (6), 3016–3028. http://dx.doi.org/10.1016/j.eswa.2014.11.057.

Pandit, R., Kolios, A., 2020. SCADA data-based support vector machine wind turbine power curve uncertainty estimation and its comparative studies. Appl. Sci. (Switzerland) 10 (23), 1–18. http://dx.doi.org/10.3390/app10238685.

Paul, V.K., Chakraborty, S., Chakraborty, S., 2022. An integrated IRN-BWM-EDAS method for supplier selection in a textile industry. Decis. Mak.: Appl. Manag. Eng. 5 (2), 219–240. http://dx.doi.org/10.31181/dmame0307102022p.

Rani, P., Mishra, A.R., Pardasani, K.R., Mardani, A., Liao, H., Streimikiene, D., 2019. A novel VIKOR approach based on entropy and divergence measures of pythagorean fuzzy sets to evaluate renewable energy technologies in India. J. Clean. Prod. 238, 117936. http://dx.doi.org/10.1016/j.jclepro.2019.117936.

Rezaei, J., 2015. Best-worst multi-criteria decision-making method. Omega 53, 49–57.

Riaz, M., Farid, H.A., 2022. Picture fuzzy aggregation approach with application to third-party logistic provider selection process. Rep. Mech. Eng. 3 (1), 318–327. http://dx.doi.org/10.31181/rme20023062022r.

Saaty, T.L., 2008. Decision making with the analytic hierarchy process. Int. J. Serv. Sci. 1 (1), 83–98, URL: https://www.rafikulislam.com/uploads/resourses/197245512559a37aadea6d.pdf.

Shields, M., Beiter, P., Nunemaker, J., Cooperman, A., Duffy, P., 2021. Impacts of turbine and plant upsizing on the levelized cost of energy for offshore wind. Appl. Energy 298, 117189. http://dx.doi.org/10.1016/j.apenergy.2021.117189.

Staffell, S.P., Pfenninger, S., 2016. Renewables ninja. URL: https://www.renewables.ninja/. (Accessed: 2023-10-12).

Statistics Norway, 2023. Electricity prices. https://www.ssb.no/en/energi-og-industri/energi/statistikk/elektrisitetspriser. Updated: 16 August 2023, Accessed: 12 October 2023.

Statnett, 2021. Havvind fra utsira og sørlige nordsjø II. URL: https://www.statnett.no/for-aktorer-i-kraftbransjen/nettkapasitet-til-produksjon-og-forbruk/tilknytning-av-havvind-fra-utsira-og-sorlige-norsjo-ii. In Norwegian. Accessed: 2023-09-07.

Statnett, 2022. Virkninger på kraftsystemet av ulike nettløsninger for utbygging av havvind i fase 2 på sørlige nordsjø iistatnett. URL: https://www.statnett.no/globalassets/havvind/2022-12-02-nve-oppdrag-om-virkninger-av-nett-til-havs---sign-002.pdf. In Norwegian. Accessed: 2023-09-07.

Taylor, P., Yue, H., Campos-Gaona, D., Anaya-Lara, O., Jia, C., 2021. Turbine layout optimisation for large-scale offshore wind farms–a grid-based method. IET Renew. Power Gener. (February), 1–17. http://dx.doi.org/10.1049/rpg2.12295, URL: https://onlinelibrary.wiley.com/doi/10.1049/rpg2.12295.

Van der Valk, P.L.C., 2014. Coupled Simulations of Wind Turbines and Offshore Support Structures: Strategies based on the Dynamic Substructuring Paradigm (Ph.D. thesis). TU Delft, http://dx.doi.org/10.4233/uuid:ac619319-9eae-443d-8b94-d0246f80ffdb.

Vermeer, L., Sørensen, J.N., Crespo, A., 2003. Wind turbine wake aerodynamics. Prog. Aerosp. Sci. 39 (6–7), 467–510. http://dx.doi.org/10.1016/S0376-0421(03)00078-2.

Wang, C.-N., Nguyen, N.-A.-T., Dang, T.-T., 2022. Offshore wind power station (OWPS) site selection using a two-stage MCDM-based spherical fuzzy set approach. Sci. Rep. 12 (1), 4260. http://dx.doi.org/10.1038/s41598-022-08257-2.

Wind, P., 2023. OPEX benchmark: An insight into operational expenditures of European offshore wind farms. URL: https://peak-wind.com/insights/opex-benchmark-an-insight-into-operational-expenditures-of-european-offshore-wind-farms/. Accessed: 2023-03-16.

Yazdi, M., Nedjati, A., Zarei, E., Abbassi, R., 2022. Application of multi-criteria decision-making tools for a site analysis of offshore wind turbines. In: Artificial Intelligence and Data Science in Environmental Sensing. Elsevier, pp. 109–127. http://dx.doi.org/10.1016/B978-0-323-90508-4.00008-3.

Yin, C., Ji, F., Weng, X., Zhang, Q., Geng, S., 2021. The optimal plan selection framework of rail transit photovoltaic power station under probabilistic linguistic environment. J. Clean. Prod. 328, 129560. http://dx.doi.org/10.1016/j.jclepro.2021.129560.

Yu, Y., Wu, S., Yu, J., Chen, H., Zeng, Q., Xu, Y., Ding, H., 2022a. An integrated MCDM framework based on interval 2-tuple linguistic: A case of offshore wind farm site selection in China. Process Saf. Environ. Prot. 164, 613–628. http://dx.doi.org/10.1016/j.psep.2022.06.041.

Yu, Y., Wu, S., Yu, J., Xu, Y., Song, L., Xu, W., 2022b. A hybrid multi-criteria decision-making framework for offshore wind turbine selection: A case study in China. Appl. Energy 328, 120173. http://dx.doi.org/10.1016/j.apenergy.2022.120173.

Zavadskas, E.K., Turskis, Z., Antucheviciene, J., Zakarevicius, A., 2012. Optimization of weighted aggregated sum product assessment. Elektron. Elektrotech. 122 (6), 3–6.

Zhang, L., Li, Y., Xu, W., Gao, Z., Fang, L., Li, R., Ding, B., Zhao, B., Leng, J., He, F., 2022. Systematic analysis of performance and cost of two floating offshore wind turbines with significant interactions. Appl. Energy 321, 119341. http://dx.doi.org/10.1016/j.apenergy.2022.119341.

Zhang, X.-y., Wang, X.-k., Yu, S.-m., Wang, J.-q., Wang, T.-l., 2018. Location selection of offshore wind power station by consensus decision framework using picture fuzzy modelling. J. Clean. Prod. 202, 980–992. http://dx.doi.org/10.1016/j.jclepro.2018.08.172, URL: https://www.sciencedirect.com/science/article/pii/S0959652618325150.